

AD-A078 686

BATTELLE COLUMBUS LABS OH
METHODOLOGY FOR MAKING A SELF-ABSORPTION CORRECTION TO THE SIMP--ETC(U)
OCT 79 A A BOIARSKI

F/G 20/13

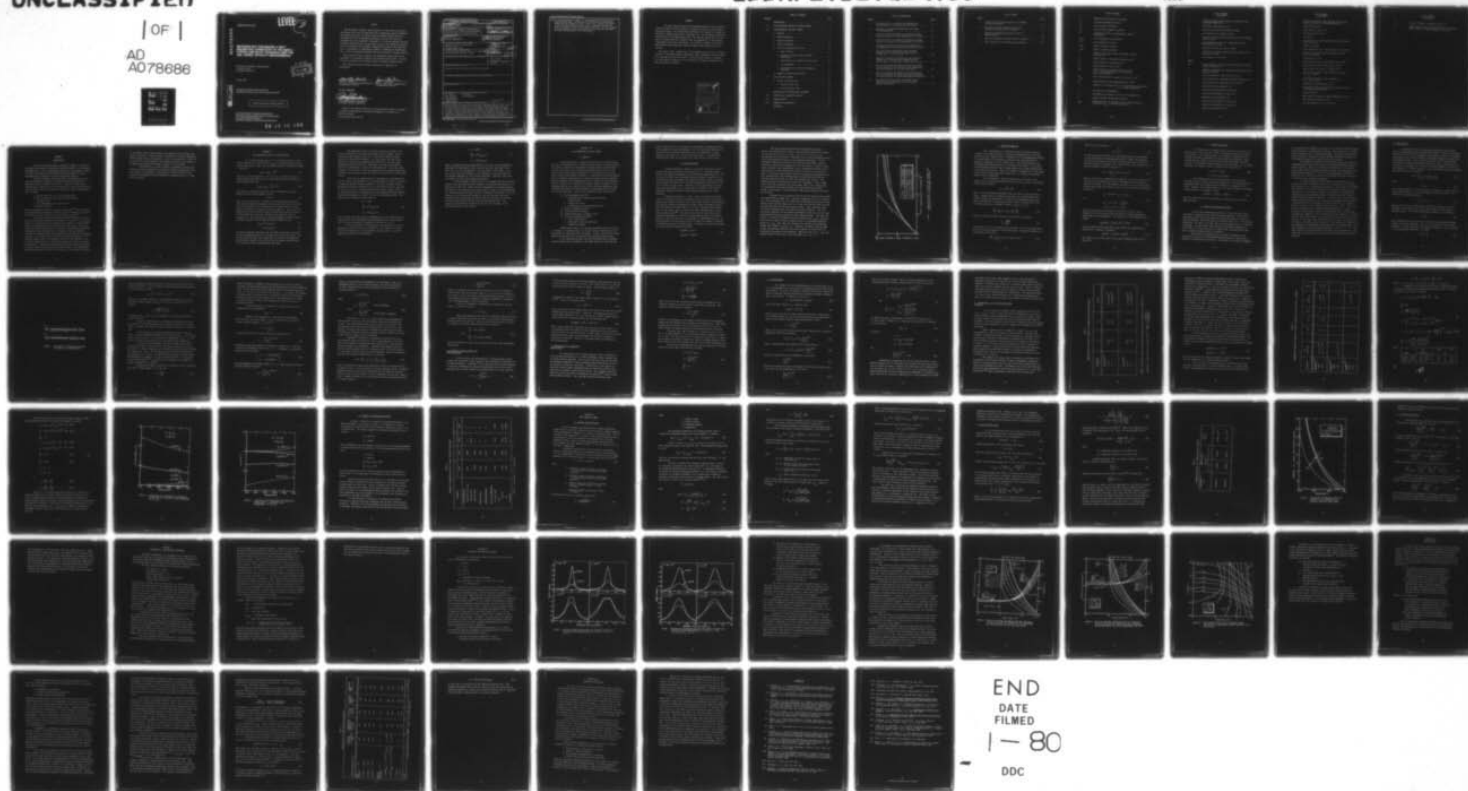
F33615-76-C-3145

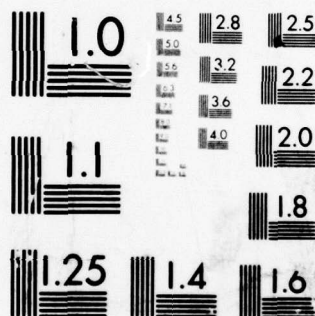
AFDNI -TD-79-3122

UNCLASSIFIED

| OF |

AD
A078686





MICROCOPY RESOLUTION TEST CHART
NATIONAL BUREAU OF STANDARDS-1963-A

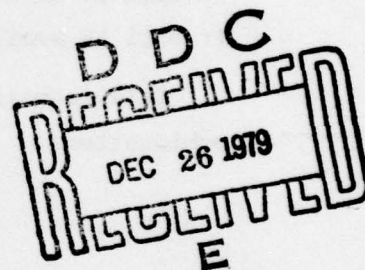
ADA 078686

AFFDL-TR-79-3122

LEVEL 2

**METHODOLOGY FOR MAKING A SELF-
ABSORPTION CORRECTION TO THE SIMPLE
COPPER-LINE-RATIO TECHNIQUE USED FOR
ARC-TUNNEL ENTHALPY MEASUREMENTS**

*BATTELLE'S COLUMBUS LABORATORIES
505 KING AVENUE
COLUMBUS, OHIO 43201*



October 1979

DDC FILE COPY

TECHNICAL REPORT AFFDL-TR-79-3122
Final Report for period October 1977 through October 1978

Approved for public release; distribution unlimited.

AIR FORCE FLIGHT DYNAMICS LABORATORY
AIR FORCE WRIGHT AERONAUTICAL LABORATORIES
AIR FORCE SYSTEMS COMMAND
WRIGHT-PATTERSON AIR FORCE BASE, OHIO 45433

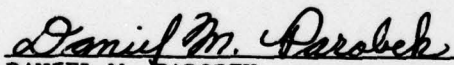
79 12 18 096

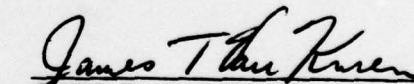
NOTICE

When Government drawings, specifications, or other data are used for any purpose other than in connection with a definitely related Government procurement operation, the United States Government thereby incurs no responsibility nor any obligation whatsoever; and the fact that the Government may have formulated, furnished, or in any way supplied the said drawings, specifications, or other data, is not to be regarded by implication or otherwise as in any manner licensing the holder or any other person or corporation, or conveying any rights or permission to manufacture, use, or sell any patented invention that may in any way be related thereto.

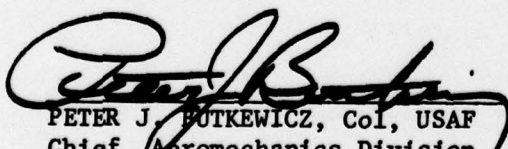
This report has been reviewed by the Information Office (IO) and is releasable to the National Technical Information Service (NTIS). At NTIS, it will be available to the general public, including foreign nations.

This technical report has been reviewed and is approved for publication.


DANIEL M. PAROBEC
Tech Mgr, Experimental Engineering Br
Aeromechanics Division


JAMES T. VAN KUREN
Chief, Experimental Engineering Br
Aeromechanics Division

FOR THE COMMANDER


PETER J. BUTKEWICZ, Col, USAF
Chief, Aeromechanics Division
AF Flight Dynamics Laboratory

Copies of this report should not be returned unless return is required by security considerations, contractual obligations, or notice on a specific document.

19 REPORT DOCUMENTATION PAGE		READ INSTRUCTIONS BEFORE COMPLETING FORM	
1. REPORT NUMBER AFFDL-TR-79-3122	2. GOVT ACCESSION NO.	3. RECIPIENT'S CATALOG NUMBER 9	
4. TITLE (and Subtitle) Methodology for Making a Self-Absorption Correction to the Simple Copper-Line-Ratio Technique Used for Arc-Tunnel Enthalpy Measurements	5. TYPE OF REPORT & PERIOD COVERED Final rept. October 1977-October 1978		
7. AUTHOR(s) Anthony A. Boiarski	6. PERFORMING ORG. REPORT NUMBER		
	8. CONTRACT OR GRANT NUMBER(s) 33615-76-C-3145 P.O. RI-83218		
9. PERFORMING ORGANIZATION NAME AND ADDRESS Battelle's Columbus Laboratories / 505 King Avenue Columbus, Ohio 43201	10. PROGRAM ELEMENT, PROJECT, TASK AREA & WORK UNIT NUMBERS 62201F; 2404; 240413; 24041302		
11. CONTROLLING OFFICE NAME AND ADDRESS Air Force Flight Dynamics Laboratory (AFFDL/FXN) Wright-Patterson AFB, Ohio 45433	12. REPORT DATE October 1979		
14. MONITORING AGENCY NAME & ADDRESS (if different from Controlling Office)	13. NUMBER OF PAGES 77		
	15. SECURITY CLASS. (of this Report) Unclassified		
15a. DECLASSIFICATION/DOWNGRADING SCHEDULE			
16. DISTRIBUTION STATEMENT (of this Report) Approved for public release; distribution unlimited.			
17. DISTRIBUTION STATEMENT (of the abstract entered in Block 20, if different from Report)			
18. SUPPLEMENTARY NOTES			
19. KEY WORDS (Continue on reverse side if necessary and identify by block number) Arc Tunnel Line Shift Flow Enthalpy Line Broadening Self-Absorption Copper Spectra Copper Density			
20. ABSTRACT (Continue on reverse side if necessary and identify by block number) Detailed theory and analytical procedures are presented which provide a method for self-absorption correction of the simple 5106/5153 Å copper-line-ratio technique used to measure arc-tunnel stagnation enthalpy. This correction procedure involves simultaneous measurement of the 5106 Å line full half-width in order to infer copper number density and gas temperature from the self-absorption broadened line profile shape, and the simple line intensity ratio. Theoretical formulations of other dominant line-broadening contributions (i.e., Doppler, Van der Waals, and Stark effects) are also included in order to			

407 080

JOD

20. accurately determine the degree of line broadening that results from self-absorption alone. Typical data reduction curves are presented to demonstrate the correction process. These curves indicate that large errors in measured enthalpy could result if self-absorption was not properly accounted for in the data analysis procedure. An error estimate is also included to indicate the typical accuracy presently obtainable from this self-absorption correction method.

FOREWORD

The work reported herein was accomplished under Air Force Contract F33615-76-C-1345 with the University of Dayton as Task 33 of the Visiting Scientist Program. The research was performed by Dr. Anthony A. Boiarski of Battelle's Columbus Laboratories, Columbus, Ohio. The performance period was from October 1977 through October 1978. The work was carried out as an element of in-house Work Unit 24041302 "Real Gas Diagnostics" of Task 240413, "Aerodynamic Ground Test Technology". Mr. Daniel M. Parobek of the Experimental Engineering Branch was contractor monitor and in-house work unit engineer.

The author and Mr. Parobek wish to acknowledge the work of Mr. Jon Bader, formerly of the Flight Dynamics Laboratory, whose unpublished efforts served as a starting point for this report. Also the author wishes to recognize Mr. Clyde Mason of Battelle for his assistance in computer programming and general numerical analysis.

Accession For	
NTIS GDA&I	<input checked="checked" type="checkbox"/>
DDC TAB	<input type="checkbox"/>
Unannounced	<input type="checkbox"/>
Justification	
By _____	
Distribution/	
Availability Codes	
Dist	Avail and/or special
A	

TABLE OF CONTENTS

SECTION		PAGE
I	INTRODUCTION	1
II	SELF-ABSORPTION EFFECTS ON COPPER SPECTRA.	3
III	LINE-BROADENING AND SHIFT THEORY	6
	A. General.	6
	B. Fixed Broadening	7
	C. Doppler Broadening	10
	D. Zeeman Broadening.	12
	E. Collision Broadening and Shift	12
	1. Impact Theory.	14
	2. Validity of Impact Theory for RENT Environment.	19
	3. Modification to Lindholm's Impact Theory	20
	4. Ion Broadening	22
	5. Determination of Collision-Broadening Constants.	24
	F. Summary of Broadening and Shift.	32
IV	LINE INTENSITY THEORY.	34
	A. General Analytical Form.	34
	1. Optically-Thin Limit	38
	2. Optically-Thick Limit.	42
V	DESCRIPTION OF COMPUTATIONAL PROCEDURES.	44
VI	DISCUSSION OF ANALYTICAL RESULTS	47
VII	ERROR ESTIMATE	56
VIII	SUMMARY AND CONCLUSIONS.	62
	REFERENCES	64

LIST OF ILLUSTRATIONS

FIGURE		PAGE
1	Correction Factor to Account for Apparent Line Broadening Due to the Measurement Instrument.	9
2	Vibration of a Perturbed Oscillator (a) Lorentz (b) Lenz-Weisskopf.	15
3	Collisional Full Half-Width of Appropriate Copper Lines as a Function of Gas Temperature ($p = 80$ atm)	30
4	Line Shift Due to Collisions for Appropriate Copper Lines as a Function of Gas Temperature ($p = 80$ atm)	31
5	Integrated Line-Intensity Ratio as a Function of Gas Temperature for Optically-Thin and -Thick Limits. . . .	41
6	True Line Contour and Relative Line Intensity Changes with Increasing Copper Number Density ($p = 80$ atm, $\ell = 2$ cm, $\gamma_A = 0$).	48
7	Measured Line Contour and Relative Line Intensity Changes with Increasing Copper Number Density ($p = 80$ atm, $\ell = 2$ cm, $\gamma_{A1} = 1.64 \text{ \AA}$, $\gamma_{A2} = 1.41 \text{ \AA}$).	49
8	Ratio of Line Peak Intensities and Full Half-Width of the 5106 \AA Line as a Function of Gas Temperature and Copper Density for the True Line Shapes	52
9	Ratio of Line Peak Intensities and Full Half-Width of the 5106 \AA Line as a Function of Gas Temperature and Copper Density for Actual Experimental Conditions	53
10	Data Reduction Plots Used to Determine Copper Density and Gas Temperature from the Measured Copper Line Spectra	54

LIST OF TABLES

TABLE		PAGE
1	Constants Used by Various Authors to Determine the Collision Radius	25
2	Broadening Constants Reported by Various Authors for Copper Lines of Interest	27
3	Summary of Broadening and Shift Values for RENT Conditions.	33
4	Emission Constants for Copper Lines of Interest.	40
5	Error Analysis for Self-Absorption Correction.	60

LIST OF SYMBOLS

B	Magnetic field strength in kilogauss
C_n	Collision-broadening constant
C_4	Stark constant in cm^4/sec
C_6	Van der Waals constant in cm^6/sec
I_1	Intensity of Line 1 at wavelength λ_1 (peak or integrated)
I_{line}	Total integrated line intensity
I^p	Peak intensity of a line
$I'(\beta)$	Elastic collision constant
$I''(\beta)$	Elastic collision constant
l	Observed path length within the region of atomic emission in cm
N	Number density of radiating particles in cm^{-3}
N_e	Number density of electrons in cm^{-3}
N_I	Number density of ions in cm^{-3}
N_N	Number density of neutral particles in cm^{-3} (i.e., total number density of all neutrals used in calculations)
$N_{\text{O Cu}}$	Total number density of copper in the flow in cm^{-3}
N_p	Number density of perturbing particles in cm^{-3}
n	Indicator of collision type $n = 6$, Van der Waals interaction $n = 4$, Stark interaction
p	Gas pressure in atmospheres
R	Universal gas constant ($R = 8.317 \times 10^7 \text{ erg/mole } ^\circ\text{K}$)
r	Distance between interacting particles
r_{min}	Minimum distance of approach of two particles during an interaction ($r_{\text{min}} \equiv$ collision radius, ρ_c)

LIST OF SYMBOLS
(Continued)

T	Period of uninterrupted emission in Lorentz's line-broadening model in sec
T	Gas kinetic temperature in °K
v_e	Electron velocity in the plasma in cm/sec
v_I	Ion velocity in a plasma in cm/sec
v_N	Velocity of natural particles relative to the emitting atom in cm/sec
\bar{v}_p	Most probable velocity for a Maxwellian velocity distribution in cm/sec
v_p	Relative collision velocity in cm/sec
v_s	Velocity of a particle along the line of sight of an observer in cm/sec
Z	Ion charge ($Z = 1$ for NO^+)
<u>Greek</u>	
α_n	Fourier analysis parameter used in effective collision radius calculations
β	Elasticity parameter for collisions with given emitting states of an atom
γ	Full half-width of a line (in sec^{-1} or Å)
γ_A	Full half-width of instrument apparatus function in Å
γ_6	Van der Waals full half-width of a line in Å
γ_c	Collisional full half-width in Å
γ_D	Doppler full half-width of a line in Å
γ_F	Fixed full half-width of a line in Å
γ_m	Measured full half-width in Å
γ_Z	Zeeman full half-width of a line in Å
γ_4	Stark full half-width of a line in Å
Δ	General line shift in sec^{-1}

LIST OF SYMBOLS
(Continued)

ΔE	Distance between the atomic emitting state and the nearest state able to exchange energy with it
$\Delta \omega$	Phase shift in sec^{-1}
Δ_4	Stark shift of a line in \AA
Δ_6	Van der Waals shift in \AA
$\Delta \lambda$	Line shift
$\Delta \lambda_p$	Line shift due to emitter motion at the most probable velocity atom, v_p
$\Delta \lambda_s$	Doppler line shift
η	Total phase shift due to an atom particle interaction
η_0	Phase shift constant used in effective collision radius calculations
λ	Wavelength in cm or \AA
μ_A	Atomic mass per mole of the emitting atom in AMU's
μ_{Cu}	Atomic mass per mole of copper ($\mu_{\text{Cu}} = 63.56$)
μ_e	Electron mass per mole ($\mu_e = 5.4876 \times 10^{-4}$)
μ_N	Atomic mass per mole of neutral particles (assume $\mu_N \approx \mu_{\text{N}_2} = 28.024$)
μ_I	Atomic mass per mole of most predominant ion ($\mu_I = \mu_{\text{NO}^+} = 30.02$)
ν	Frequency of line radiation in sec^{-1}
ρ_0	Effective collision radius or optical collision radius or Weisskopf collision radius
ρ_c	Collision radius
τ_r	Mean radiative lifetime of atomic emission line in sec
τ_c	Time between collisions in sec
ω	Circular frequency ($\omega = 2 \pi \nu$) in sec^{-1}

LIST OF SYMBOLS
(Continued)

ω_0

Circular frequency of unshifted line center

Ω

Quantity used to check the applicability of utilizing
impact theory for line-broadening calculations

SECTION I

INTRODUCTION

The Air Force Flight Dynamics Laboratory (AFFDL) is involved in development and testing of techniques to measure enthalpy in an arc-heated wind-tunnel flow. One of these methods employs the spectroscopic analysis of copper line radiation associated with an unknown amount of copper contaminant that is present in the high-temperature effluent.

Several exploratory studies have been performed using this non-obtrusive diagnostic technique to measure stagnation enthalpy in the AFFDL Reentry Nose Tip (RENT) Facility⁽¹⁻⁷⁾. Results of these efforts indicated that a simple ratio of the intensities of lines at 5106 and 5153 Å could be used to infer gas temperature provided that the following assumptions are made:

- Optically-thin gas (i.e., no self-absorption)
- Uniform temperature and copper density along the observation path
- Local Thermodynamic Equilibrium (LTE)
- Constant pressure.

The first assumption was found to be most restrictive^(6,7) and theoretical investigations were undertaken at AFFDL to provide a method for correcting the simple line-ratio technique for self-absorption effects⁽⁶⁾.

This report presents the analytical methods required to make the above correction and associated error estimate. In Section II, the general aspects of self-absorption are discussed with reference to overall methodology for accomplishing the correction of this error source. Section III provides a detailed discussion of the myriad of line-broadening mechanisms and associated theoretical models. The equation forms and empirical constants are presented which provide methods of calculating the broadening and shift of the copper lines of interest for RENT flow conditions. Line intensity profile theory is discussed in Section IV with emphasis on the so-called "Voight Profile" for predicting detailed line shape for varying copper density. Integrated line-intensity formulations are also presented for special cases of optically-thin and -thick limits. The computational methods are presented in Section V and results of the computer calculations

of line shape, width, peak intensity, and integrated line intensity are given in Section VI. Copper density is treated as a separate independent variable along with gas temperature, so the plots generated in Section VI can be used to correct measured line-intensity ratios for the presence of an unknown and uncontrolled amount of copper in the test gas.

In Section VII, an error estimate is provided to indicate the accuracy of this self-absorption correction procedure assuming all other error sources are negligible. The estimate is based on typical data obtained in the RENT gas-cap environment for peaked-profile (i.e., high-swirl) operation.

SECTION II

SELF-ABSORPTION EFFECTS ON COPPER SPECTRA

For an optically-thin gas (i.e., no self-absorption) the integrated intensity of an emission line, I_{line} , is a linear function of total copper number density, N_{Cu} , and the observed length of the emission region, ℓ , such that

$$I_{\text{line}} = N_{\text{Cu}} \ell f(T) \quad (1)$$

where T is the gas temperature. For this case, the temperature can be determined by using a simple ratio of two emission lines to eliminate all other variables such that

$$I_{\text{line}_1} / I_{\text{line}_2} = \frac{I_1}{I_2} = f(T) \quad (2)$$

The width, γ , of these optically-thin lines is independent of copper density and optical path length such that

$$\gamma = f(T, p) \quad (3)$$

where p is the gas pressure. However, as the copper density increases, line radiation emitted by thermally excited copper atoms from a particular point in the plasma can be reabsorbed by other copper atoms in a lower energy state before the radiation reaches the observer. The center of an emission line is most affected; hence, self-absorption causes an increase in the measured line width and a decrease in the measured line peak intensity, I^p . The line width and integrated intensity therefore become nonlinear functions of copper density and path length such that

$$I_{\text{line}} = f(T, p, N_{\text{Cu}}, \ell) \quad (4)$$

$$\gamma = f(T, p, N_{\text{Cu}}, \ell) \quad (5)$$

For those transitions associated with the atomic ground state, inversion of the line-intensity profile can actually occur at the line center. But, for the particular upper state transitions of interest, self-absorption simply causes a change in line contour from its original Gaussian shape to a flat-top line with Gaussian-shaped line wings.

Self-absorption would not be such a difficult problem if the shape and intensity of all lines were nearly equally changed. However, the more intense emission lines (i.e., lines with a higher strength factor) are affected more strongly. For this reason, the 5106 Å line displays the effects of self-absorption sooner (i.e., at lower copper densities) than the 5153 Å line. Therefore, the ratio of the 5106 to 5153 Å line intensities is altered by self-absorption. Since this line-intensity ratio is used to infer gas temperature, the apparent temperature obtained from the measured line ratio must be corrected for self-absorption effects.

There are two common methods of correcting for self-absorption, and both involve determination of the unknown amount of copper in the flow by measuring another dependent parameter. The first technique involves measuring the absolute intensity of one of the lines as well as the ratio of the two lines for a fixed pressure and optical path length. This is an acceptable method but cumbersome since any technique involving absolute intensity measurements is subject to a host of measurement errors. The method can be represented analytically as

p, ℓ - fixed

$$\frac{I_1}{I_2} = f(T, N_{\text{Cu}}, p, \ell) \quad (6)$$

$$I_1 = f(T, N_{\text{Cu}}, p, \ell) \quad .$$

Hence, we have two equations and two unknowns so the gas temperature and copper density can be determined from measurements of the line-intensity ratio I_1/I_2 and the absolute intensity of one line (i.e., I_1).

The second method of correcting for self-absorption is to take advantage of the fact that the line width is also a function of copper density and temperature at fixed pressure and path length. The set of equations can then be written whereby

p, ℓ - fixed

$$\frac{I_1}{I_2} = f(T, N_{\text{O}_{\text{Cu}}}, p, \ell) \quad (7)$$

$$\gamma_1 = f(T, N_{\text{O}_{\text{Cu}}}, p, \ell) \quad .$$

Again, the temperature and copper density of the gas can be determined by measuring the line-intensity ratio and, in this case, the width of one line (i.e., γ_1) is also measured. The line width, or full width of the line at half the peak intensity, is not dependent on the value used for the absolute magnitude of the line peak intensity. Therefore, less error will result for this latter method of analysis.

In both methods outlined above, it is presumed that the functional forms for the line width and line intensity can be given analytically [i.e., Equations (4) and (5)]. These functional dependencies are required before line width or line intensity data can be used to correct for self-absorption. The resulting correction simply involves accounting for how much of the line-intensity ratio, the absolute intensity, and the line width are due to temperature and pressure effects and how much are caused by the presence of excess copper atoms along the known optical emission path. The analytical representation of these effects will be the subject of the following sections of this report.

SECTION III

LINE BROADENING AND SHIFT THEORY

A. General

Shape and position of spectral lines emitted from various atomic species in a plasma have been a subject of great interest to spectroscopists. As a result, a good deal of experimental and theoretical effort has been devoted to the field. This interest is motivated by the fact that line width and shift information, accompanied by line-intensity data, can be used to infer various plasma properties. In particular, an accurate measurement of stagnation temperature in the RENT environment cannot be obtained without considering line broadening in order to correct for self-absorption effects. However, the problem of developing a general treatment of line broadening and shift is complicated by the fact that many mechanisms simultaneously exist which can cause broadening and wavelength shift of lines in a plasma environment. These various mechanisms can be classified as

- (1) Fixed broadening and shift
 - a. Broadening due to hyperfine structure and isotope shift
 - b. Natural line width
 - c. Broadening due to the measurement device
- (2) Doppler broadening and shift
- (3) Self-absorption broadening
- (4) Zeeman broadening in a magnetic field
- (5) Collision broadening and shift
 - a. Van der Waals effect
 - b. Stark effect (ions and electrons)
 - c. Resonance processes.

Simultaneous action of all the above mechanisms makes it difficult to evaluate, in a general manner, the relative role of each process on the total width of a particular line of interest. Further, each line will behave differently even when the line originates from the same plasma species.

In the following sections, the above mechanisms will be examined in greater detail with an emphasis on the shape and shift of the 5106 and

5153 Å copper lines in an arc-heated gas containing an unknown and uncontrolled amount of copper contaminant. At first, particular emphasis will be placed on the broadening mechanisms that are independent of copper density in the flow (i.e., the optically-thin limit). Self-absorption broadening will then be the subject of a later section of this report.

B. Fixed Broadening

Fixed broadening is common to all spectral lines and is due to natural line width, hyperfine line structure (i.e., including isotopic shifts), and apparent broadening caused by the measurement apparatus. For the case of natural line broadening, external fields are neglected (i.e., isolated atom) and Heisenberg's uncertainty principle is used to estimate the resulting line width due to the quantum mechanical uncertainty in the value of atomic energy levels. Results of these calculations show that the natural line width, γ_N , is of the order of 0.0001 Å. This width is negligible compared with other line-broadening mechanisms and can be neglected.

Hyperfine structure of a line is due to the fact that a given "line" can actually be made up of several close but separate transitions. Nuclear spin effects and isotope shift cause this multiple line phenomenon; and when the intensity distribution of these various components overlap, they can dominate the fixed width of the line. High-resolution measurements of the copper lines of interest have been obtained using a copper hollow-cathode source⁽⁸⁾. The spectra show that the 5106 line is more accurately described as a triplet of equally-spaced peaks, 0.02 Å apart. Hence, the 5106 line will have a fixed width of approximately 0.04 Å. On the other hand, the 5153 Å line is truly a single line having no evidence of hyperfine structure or isotope shift. In summary, the true fixed width, γ_F , of the lines of interest is given by

$$\begin{aligned}\gamma_F(5106) &= 0.04 \text{ Å} \\ \gamma_F(5153) &= 0.0001 \text{ Å} \quad .\end{aligned}\tag{8}$$

The above fixed width would not be measured in practice because the apparatus used to make a line-width measurement will normally add some apparent width to the line. This is due to the fact that the measured line is actually a convolution of the true line shape with the finite width apparatus function of the measuring instrument. If the instrument apparatus function has an infinitely-narrow width, then the convoluted profile would represent the true line profile. Within certain limits, apparent line broadening due to the experimental apparatus can be subtracted out of the measured line profile to arrive at the true line width. This correction procedure involves determining the apparatus function experimentally, then deconvoluting the measured profile with the apparatus-function profile to obtain the original line contour. The apparatus function is measured by using that instrument to scan a light source that emits radiation with ultra-narrow lines (i.e., source lines are approximately 100 times narrower than apparatus-function width). Lasers, pen-ray lamps, or hollow-cathode light sources produce such ultra-narrow lines.

Provided that the apparatus function and the measured line profile have characteristic shapes (i.e., Gaussian, triangular, etc.), the convolution can be performed once for various full half-widths and then correction curves can be used from that point on to infer the true line width from the measured width and the apparatus-function width. Such correction curves for several characteristic line shapes are shown in Figure 1. For the particular conditions of the present experimental setup, both the true line and apparatus-function profiles are nearly Gaussian shaped. The true line width, γ , can then be determined from the measured width, γ_m , by using the solid curve in Figure 1 given a measured value of the apparatus-function width (i.e., γ_A). Note that the correction for apparent line broadening becomes quite large for $\gamma_A/\gamma_m > 0.5$. Therefore, an effort should be made to keep the apparatus function as narrow as possible to avoid errors in correcting for apparent line broadening. Below the value of $\gamma_A \approx \gamma_m/3$, the measured width is very close to the true width (i.e., $\gamma_m \approx \gamma$).

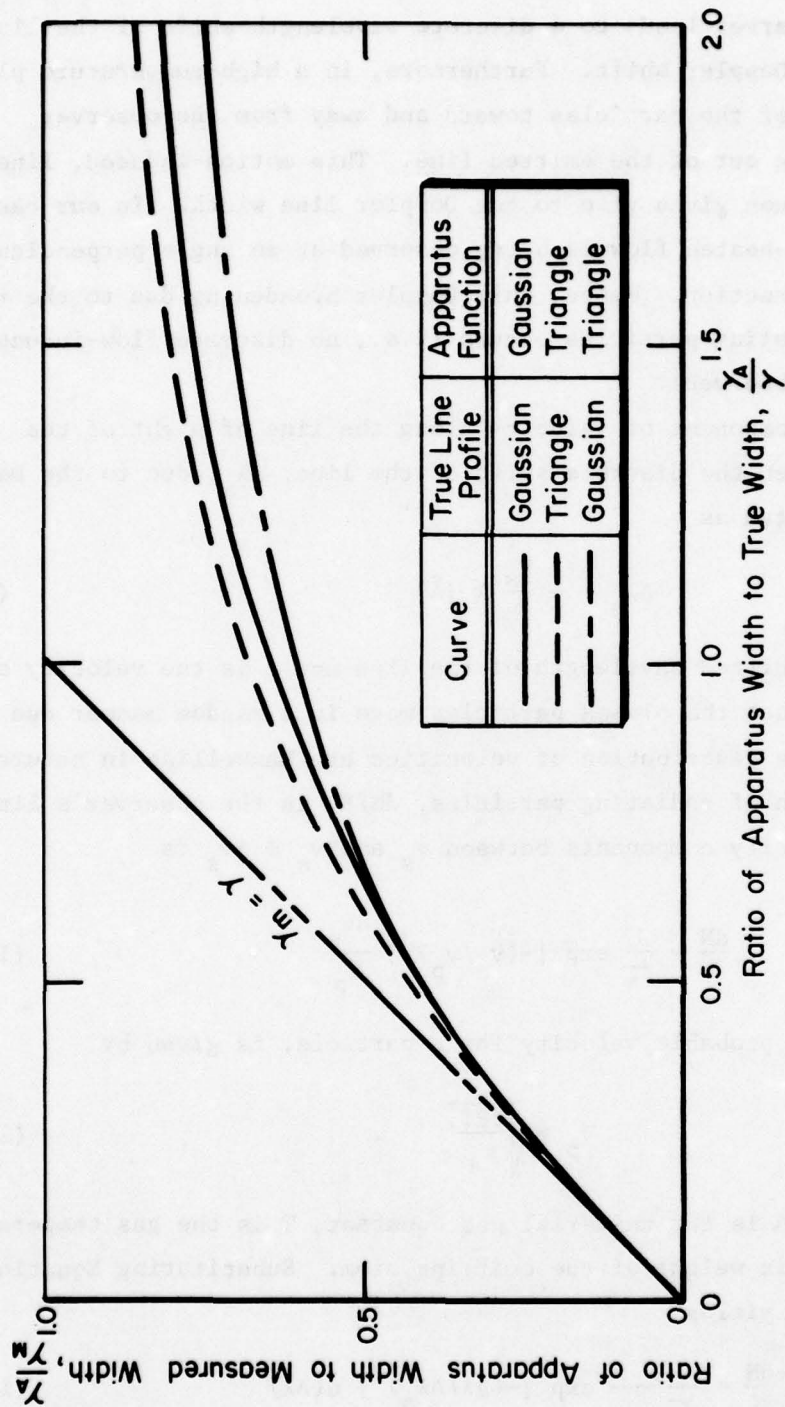


FIGURE 1. CORRECTION FACTOR TO ACCOUNT FOR APPARENT LINE BROADENING DUE TO THE MEASUREMENT APPARATUS

C. Doppler Broadening

The steady motion of a radiating particle along the direction of sight of an observer leads to a discrete wavelength shift of the line which is called a Doppler shift. Furthermore, in a high-temperature plasma, the random motion of the particles toward and away from the observer produces a smearing out of the emitted line. This motion-induced, line-broadening phenomenon gives rise to the Doppler line width. In our case, the high-speed arc-heated flow is being observed at an angle perpendicular to the gas flow direction. Hence, only Doppler broadening due to the random motion of the radiating particles occurs (i.e., no discrete flow-induced Doppler shift is observed).

If the component of velocity along the line of sight of the observer is v_s , then the discrete shift of the line, $\Delta\lambda_s$, due to the Doppler effect can be written as

$$\Delta\lambda_s = \pm \frac{v_s}{c} \lambda \text{ [\AA]} \quad (9)$$

where λ is the unshifted wavelength of the line and c is the velocity of light. Assuming that the plasma particles move in a random manner due to thermal energy, the distribution of velocities are Maxwellian in nature. Hence, the fraction of radiating particles, dN/N , in the observer's line of sight with velocity components between v_s and $v_s + \Delta v_s$ is

$$\frac{dN}{N} = \frac{1}{\sqrt{\pi}} \exp [-(v_s/v_p)^2] \frac{dv_s}{v_p} \quad (10)$$

where v_p , the most probable velocity for a particle, is given by

$$v_p = \sqrt{\frac{2RT}{\mu_A}} \quad (11)$$

In Equation (11), R is the universal gas constant, T is the gas temperature, and μ_A is the atomic weight of the emitting atom. Substituting Equation (9) into Equation (10) yields

$$\frac{dN}{N} = \frac{1}{\sqrt{\pi} \Delta\lambda_p} \exp [-(\Delta\lambda/\Delta\lambda_p)^2] d(\Delta\lambda) \quad (12)$$

where now $\Delta\lambda_p$ is defined by

$$\Delta\lambda_p = \frac{\bar{v}_p}{c} \lambda \quad (13)$$

For optically-thin conditions, the line intensity will be proportional to the concentration of radiating particles, N . Hence, the intensity emitted in the interval $I(\Delta\lambda) d(\Delta\lambda)$ is proportional to the fraction of particles dN given in Equation (12). Therefore, the line intensity for a Doppler-broadened line can be written as

$$I(\Delta\lambda) = \frac{I_t}{\sqrt{\pi} \Delta\lambda_p} \exp [-(\Delta\lambda/\Delta\lambda_p)^2] \quad (14)$$

where I_t is the total integrated line intensity. The form of Equation (14) indicates that broadening due purely to the Doppler effect results in a Gaussian line shape. The full width of this line (i.e., the total width between points where the intensity falls to half its value at the maximum) is given by

$$\gamma_D = 2(\ln 2)^{1/2} \Delta\lambda_p = 1.66 \Delta\lambda_p \quad (15)$$

or

$$\gamma_D = 7.16 \times 10^{-7} \lambda \sqrt{\frac{T}{\mu_A}} [\text{\AA}]$$

λ in \AA , T in $^\circ\text{K}$, μ in AMU

where γ_D is defined as the Doppler full width of the line. From Equation (15), it can be seen that this effect is most pronounced for light atoms at high temperature. For copper, $\mu_A = 63.56$, Equation (15) yields

$$\gamma_D(\text{copper}) = 8.98 \times 10^{-8} \lambda \sqrt{T} [\text{\AA}] \quad (16)$$

The line width for the copper lines near 5100 \AA , and a temperature of interest (i.e., 6000 K), is given by

$$\gamma_D(5106) \approx \gamma_D(5153) = 0.036 \text{\AA} \quad (17)$$

This width is of the same order as the fixed broadening value for the 5106 line.

D. Zeeman Broadening

In the presence of a magnetic field, an atomic line splits into several lines. This splitting is small and symmetric about the original line position. The resulting effect is to produce a broadening of the original line when the multiplet is viewed under low resolution. Exact calculations are complex, but an estimate can be made which is fairly accurate. This estimate indicates that the line full-width, γ_z , for Zeeman broadening in a magnetic field of strength B can be written as

$$\gamma_z \approx 10^{-9} \lambda^2 B [\text{\AA}] \quad (18)$$

λ in \AA , B in kilogauss.

In the RENT facility, two coils are used to rotate the arc attachment point in order to extend electrode life. The coil nearest the measurement point has a magnetic field strength of 2 kilogauss at its center. However, at the measurement point, the field strength has decreased to approximately 0.1 kilogauss. Hence,

$$\gamma_z(5106) \approx \gamma_z(5153) \approx 0.0026 \text{\AA} \quad (19)$$

This is a small effect and can, therefore, be neglected for the present RENT conditions.

E. Collision Broadening and Shift

In this case, broadening and shift of a line occur due to the interaction of radiating atoms with surrounding particles. For a plasma environment, these interacting particles could be electrons or ions (i.e., Stark broadening), neutral molecules or nonsimilar atoms (i.e., Van der Waals broadening), and atoms of the same kind as the emitting atom (i.e., resonance broadening). In the present case, radiation from copper contaminant in arc-heated air is being considered so copper-copper interactions are rare. Hence, resonance broadening will be neglected.

The analytical representation of collision broadening is the most difficult of all the broadening mechanisms because it involves the modeling of atom-particle interactions. Furthermore, the overall broadening

of a particular line depends on the type of atom and the particular energy states involved in the radiating transition. The formulation also depends on the particular type of interacting partner. Hence, much more experimental evidence is required to obtain empirical broadening constants and to validate the theory for a particular line of interest.

The analytical solution to the problem of predicting collision broadening can be set up on the basis of the quantum-mechanical theory of atomic collision. However, the results of quantum theory calculations nearly always agree with simple formulations that can be obtained using a quasi-classical approach⁽⁹⁾. This latter approximation considerably simplifies the closed form solution to the problem and makes the process of evaluation more physically meaningful.

In quasi-classical collision theory, the interaction of the emitting atom with surrounding particles is considered as an amplitude-phase modulation of the unperturbed oscillator. The intensity distribution in an emission line is then determined by performing a Fourier analysis averaged over all collisions. However, in performing the mathematical computations, certain inequalities must be fulfilled and this leads to several different regimes of interest. It can be shown that the closest particle-atom interaction creates the greatest perturbation and therefore contributes mostly to the wings of the line contour⁽¹⁰⁾. The combined action of the rest of the particles affects the line center. The closest particle interactions are considered best represented by a general statistical theory approach while the interactions due to longer range encounters are amenable to the so-called impact theory methods. It should be noted that neither theory can be strictly applied over the whole line profile. In the wings, the statistical theory is always valid; and at the line center, the impact theory holds true. The impact theory computations are simplified by assuming that the atom-particle interaction time, τ_I , is short compared to the time between collisions, τ_c (i.e., $\tau_I \ll \tau_c$). The impact theory is therefore strictly valid only for low pressures. On the other hand, the statistical theory is strictly valid only for very high pressures.

1. Impact Theory

As discussed above, the intensity distribution near the line center is represented by the so-called impact theory. The basic principles behind this theory of line broadening were proposed by Lorentz. He assumed the emission of an atomic oscillator is interrupted during a collision with perturbing particles. After a collision, emission at the same frequency resumed with no emission during the interaction. Hence, vibration of the oscillator is represented by a series of sinusoidal segments of duration τ (see Figure 2a). A Fourier analysis of such oscillations gives the following expression for the line intensity:

$$I(\omega) = \frac{1}{\pi\tau_r} \frac{1}{(\omega_0 - \omega)^2 + (1/\tau_r)^2} \quad (20)$$

where

$$\omega = 2\pi\nu \quad (21)$$

In the above equations, ν is the frequency of radiation, τ_r the mean radiation lifetime, and ω_0 the circular frequency of the line center. The intensity is normalized such that

$$\int_{-\infty}^{\infty} I(\omega) d\omega = 1 \quad (22)$$

Equation (20) is the so-called Lorentz dispersion formula for collision broadening. The shape of the line is often called a Lorentz shape or dispersion shape. The collision-broadening constant, γ_c , is defined by

$$\gamma_c = \frac{2}{\tau_r} \quad (23)$$

which represents the full width of the line at half the maximum intensity in units of circular frequency. Now, τ_r can be related to the collision frequency, z , if we assume that the radiative lifetime, τ_r , is of the order of the time between collisions, τ_c . Hence,

$$z = \frac{1}{\tau_c} \approx \frac{1}{\tau_r} \quad (24)$$

Thus, by defining an effective collision cross section, σ_c , the collisional half-width, γ_c , can be related to plasma properties using ordinary collision theory to obtain

$$\gamma_c = \frac{1}{2} \frac{N_p}{N_e} \frac{v_{Te}}{v_p} \left(\frac{1}{v_p} + \frac{1}{v_{Te}} \right) \quad (23)$$

where N_p is the number density of the perturbing particles, v_p is the effective collision radius, and v_{Te} is the relative collision velocity. It is given by

$$v_p = \sqrt{\frac{4\pi N_p e^2}{m_e} \left(\frac{1}{v_p} + \frac{1}{v_{Te}} \right)} \quad (24)$$

in Equation (23). v_p and v_{Te} are the weights of the colliding partners in the plasma mass.

Since the number density of perturbers is proportional to the gas pressure, P , the collisional half-width, γ_c , should be proportional to P . The collisional half-width, γ_c , is sometimes used.

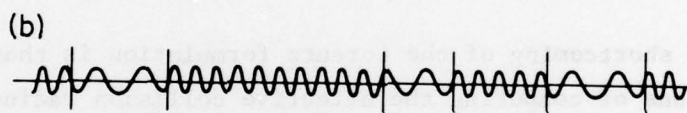
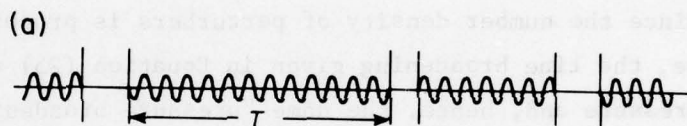


FIGURE 2. VIBRATION OF A PERTURBED OSCILLATOR
(a) LORENTZ (b) LENZ-WEISSKOPF

Thus, by defining an effective collision cross section, $\pi \rho_c^2$, the collisional half-width, γ_c , can be related to plasma properties using ordinary collision theory to obtain

$$\gamma_c = \frac{2}{\tau_c} = 2\pi \rho_c^2 N_p v_p [\text{sec}^{-1}] \quad (25)$$

where N_p is the number density of the perturbing particles, ρ_c is the effective collision radius, and v_p , the relative collision velocity, is given by

$$v_p = \sqrt{\frac{8RT}{\pi} \left(\frac{1}{\mu_1} + \frac{1}{\mu_2} \right)} \quad (26)$$

In Equation (26), μ_1 and μ_2 are the weights of the colliding partners in atomic mass units.

Since the number density of perturbers is proportional to the gas pressure, the line broadening given in Equation (25) would be proportional to pressure and, hence, the name "pressure broadening" is sometimes used.

A shortcoming of the Lorentz formulation is that it does not define a means of computing the effective collision radius, ρ_c , for various types of interactions (i.e., atom-electron, atom-neutral, etc.). It also does not account for line shift due to the atom-particle interaction.

To rectify the shortcomings of Lorentz's simple model, Lenz⁽¹¹⁾ postulated that the oscillator did not stop emitting during a collision, but rather, a change in frequency of oscillation occurred during a collision (see Figure 2b). Hence, the colliding particles could also contribute to the broadening of a line by a so-called "phase altering" collision without extinguishing the radiation. In this interaction process, as visualized by Lenz and Weisskopf⁽¹²⁾, a collision acts to detune (i.e., broaden the frequency spectrum) of a radiator.

Following this model, a particle at a distance r from a radiating atom causes a phase change, $\Delta\omega$, of the form

$$\Delta\omega = \frac{2\pi c n}{r^n} \quad (27)$$

where the exponent n depends on the particular type of force law which represents the interaction between the perturbing particle and the radiating atom. In the case of the Stark broadening effect, this exponent has the value of 4 and for a Van der Waals interaction, $n = 6$ is used. The constant c_n characterizes the interaction of the electric field of the perturbing particle with the particular energy level of the radiating atom. Hence, c_n can vary widely for each atomic emission line and for each type of perturbing particle.

In this formulation, the distance of closest approach to the radiating atom is designated by

$$r_{\min} \equiv \rho_c \quad (28)$$

Results of the computations, following Lenz and Weisskopf, show that the total phase change, η , due to collision with a particle having an impact parameter ρ_c , is given by

$$\eta = \pi^2 \frac{c_n}{v_p \rho_c^{n-1}} \quad (29)$$

solving Equation (29) in terms of the impact parameter we get

$$\rho_c = \left(\frac{\pi^2 c_n}{v_p \eta} \right)^{1/(n-1)} \quad (30)$$

According to Lenz and Weisskopf, an effective collision (i.e., one that causes line broadening) occurs for $\eta_0 > \eta \approx 1$. Therefore, η_0 divides all collisions into two kinds

$$\left. \begin{array}{ll} \eta < \eta_0 & - \text{no broadening} \\ \eta > \eta_0 & - \text{broadening} \end{array} \right\} \quad (31)$$

Lenz and Weisskopf arbitrarily picked $\eta = \eta_0 = 1$, which gives an effective collision radius of the form

$$\rho_0 = \left(\frac{\pi^2 c_n}{v_p} \right)^{1/(n-1)} \quad (32)$$

where ρ_0 is often called the Weisskopf collision radius. Also, ρ_0 is sometimes referred to as the optical radius. The full half-width in circular frequency units for the Lenz-Weisskopf collision theory is therefore given by

$$\gamma_c = 2\pi \rho_0^2 N_p v_p \quad (33)$$

where

$$\begin{aligned} \rho_0 &= \left(\frac{\pi^2 c_4}{v_p} \right)^{1/3} && \text{Stark broadening} \\ \text{and} \\ \rho_0 &= \left(\frac{\pi^2 c_6}{v_p} \right)^{1/5} && \text{Van der Waals broadening} \end{aligned} \quad (34)$$

The limit of $\eta = \eta_0 = 1$ in Lenz's theory is an approximation which results in the fact that only certain collisions are taken into account. This approximation limits Lenz's theory in principle to very low pressures and to the intensity distribution at the core of a line. However, the theory does predict a possible line shift as well as line broadening and provides a method to compute effective collision radii for various types of atom-particle interactions.

Lindholm⁽¹³⁾ succeeded in overcoming the difficulties in the Lenz-Weisskopf theory by placing no limit on the magnitude of the phase shift and by taking all phase shifts into account (i.e., both close and distant encounters are considered). Lindholm's more general theory is valid at higher pressures and over a greater portion of the line profile. It also retains the good points of Lenz's approach. Detailed calculations show that the intensity distribution is of the form

$$I(\omega) = \frac{\gamma}{2\pi} \frac{1}{(\omega - \omega_0 - \Delta)^2 + (\gamma/2)^2} \quad (35)$$

where the intensity has again been normalized to unity as in Equation (22). In Equation (35), Δ is the line shift in circular frequency units. Lindholm's analysis resulted in the similar formulation for the effective collision radius and line full half-width as given in Equations (30) and (33), respectively. However, details of the calculations show that the collision radius is actually given by

$$\rho_o = \left(\frac{\alpha_n C_n}{v_p \eta_o} \right)^{1/(n-1)} \quad (36)$$

where η_o in Equation (36) is usually set equal to 0.64 for Lindholm's theory rather than the arbitrary value of $\eta_o = 1$ for Lenz's formulation. The values of α_n are the results of detailed Fourier analyses of the collision model and C_n 's are empirical constants determined by appropriate line width measurements at known conditions.

Results of Lindholm's calculations also showed that the line shift, Δ , could be written as

$$\Delta \propto \rho_o^2 N_p v_p \quad (37)$$

Hence, from Equations (33) and (37), Lindholm's approach implies a constant magnitude of the ratio of width to shift which characterizes a definite type of interaction. Detailed calculations show that according to Lindholm's theory the width-to-shift ratio is given by

$$\frac{\gamma_4}{\Delta_4} = 1.16, \text{ (Stark)}$$

and

$$\frac{\gamma_6}{\Delta_6} = 2.8, \text{ (Van der Waals)}$$

where the subscripts 4 and 6 refer to Stark and Van der Waals broadening, respectively.

2. Validity of Impact Theory for RENT Environment

In this section, the applicability of utilizing impact theory rather than statistical theory to predict line broadening is discussed for the RENT environment. Sobel'man⁽¹⁴⁾ has shown that the collision mechanism is valid for predicting the intensity distribution near the line center provided that a certain criteria on the phase shift, $\Delta\omega$, is met such that

$$\Delta\omega \approx \gamma_c < \frac{v^{n/n-1} p}{C_n^{1/n-1}} = \Omega \quad (39)$$

For the present, Equation (39) can be simplified using Equations (33) and (36) to write the inequality in terms of the number density of perturbing particles and the optical collision radius. The resulting criterion is

$$N_p \ll \left(\frac{1}{\rho_o} \right)^3 \quad (40)$$

The Weisskopf radius for the copper lines of interest is of the order of $5 \text{ \AA}^{(15)}$. Hence, from Equation (40)

$$N_p \ll 10^{22} \text{ cm}^{-3} \quad (41)$$

must be satisfied for the impact theory to be valid in the case of collision broadening of the copper lines of interest. Calculations show that for typical RENT conditions (i.e., $P_o = 100 \text{ atm}$, $T_o \approx 6000 \text{ K}$) number density levels in the free stream and behind the bow shock wave are

$$N_p(\text{RENT}) \approx 10^{20} \ll 10^{22} \text{ cm}^{-3} \quad (42)$$

Hence, typical RENT flow conditions are such that the impact theory can be considered valid for predicting line broadening near the line center. Further evidence of the applicability of impact theory will also be provided when measured line shape, full half-width, and shift are compared to theoretical predictions. Details of the impact theory are presented in the following text.

3. Modifications to Lindholm's Impact Theory

The applicability of the quasi-classical theory of Lindholm to electron-atom interactions (i.e., Stark broadening) is more complex than the above analysis indicates. This is due to the fact that for electrons the Weisskopf mechanism for line broadening becomes less effective due to the presence of inelastic collisions. Interactions of this type (i.e., those that involve energy exchange between the collision partners) were neglected in Lindholm's semi-classical theory. More complete analytical results have been performed by Vainshtein and Sobel'man⁽¹⁶⁾ which include these inelastic effects. The resulting formulation indicates that

$$\gamma_4 = 2\pi \rho_o^2 N_e v_e I'(\beta)$$

$$\rho_o = \left(\frac{\alpha_4 C_4}{\eta_o v_e} \right)^{1/3} \quad (43)$$

$$\frac{\gamma_4}{\Delta_4} = 1.16 \frac{I'(\beta)}{I''(\beta)}$$

where $I'(\beta)$, $I''(\beta)$ are correction factors that are dependent on the elasticity parameter β which varies for each line of interest. The β parameter can be written as follows:

$$\beta \propto \frac{C_4^{1/2} (\Delta E)^{3/2}}{v_e^2} \quad (44)$$

where ΔE is the distance to the nearest energy level that can exchange energy with the original level involved in the emission line. This energy exchange between levels, which is facilitated by low ΔE 's, leads to a higher degree of inelastic interaction during atom-electron collisions.

For lines with large β values (i.e., large ΔE 's or $\beta \geq 1$), I' and I'' are approximately 1, so no correction results. However, for small β 's, I' and I'' are less than 1 with I'' falling off faster than I' . Hence, the inclusion of inelastic effects will result in slightly narrower lines and a width-to-shift ratio greater than 1.16 for the Stark broadening case.

Van der Waals broadening and shift are not affected by the above correction factors and can be written as follows:

$$\begin{aligned} \gamma_6 &= 2\pi \rho_o^2 N_N v_N \\ \rho_o &= \left(\frac{\alpha_6 C_6}{\eta_o v_n} \right)^{1/5} \\ \frac{\gamma_6}{\Delta_6} &= 2.8 \end{aligned} \quad (45)$$

4. Ion Broadening

In a plasma, the line broadening due to the Stark effect (i.e., γ_4) is determined by the interaction of an emitting atom with ions as well as electrons. For ions, the inelastic collision correction is absent for cases of practical interest because the ion velocity is small compared to that of an electron. In general, we can write

$$\gamma_4 = \gamma_4(\text{electrons}) + \gamma_4(\text{ions}) \quad (46)$$

where from impact theory [i.e., Equation (43)]

$$\gamma_4(\text{ions}) \propto v_I^{1/3} N_I \quad (47)$$

where N_I and v_I are the ion number density and velocity, respectively. For a neutral plasma, $N_e \approx N_I$, and the ion velocity can be expressed in terms of the electron velocity using Equation (26) to write

$$v_I = v_e \left(\frac{\mu_e}{\mu_I} \right)^{1/2} \quad (48)$$

where μ_e and μ_I are the electron and ion mass, respectively. Using this expression, we get the following:

$$v_I^{1/3} N_I \approx v_e^{1/3} N_e \left(\frac{\mu_e}{\mu_I} \right)^{1/6} \quad (49)$$

Hence, using Equation (43), Equation (46) can be written as

$$\gamma_4 \approx 2\pi\rho_o^2 v_e N_e [I'(\beta) + \left(\frac{\mu_e}{\mu_I} \right)^{1/6}] \quad (50)$$

where the correction for ion broadening is of the form

$$\left(\frac{\mu_e}{\mu_I} \right)^{1/6} \quad (51)$$

More exact calculations given in Reference 8 show that the actual correction factor for ion broadening is of the form

$$\left(\frac{2\mu_e z^2}{\mu_I} \right)^{1/6} \quad (52)$$

where Z is the ionic charge. Hence, the Stark broadening of a line including inelastic electron collisions and ion effects is given by

$$\gamma_4 = 2\pi\rho_o^2 v_e N_e [I'(\beta) + \left(\frac{2\mu_e Z^2}{\mu_I}\right)^{1/6}]$$

$$\rho_o = \left(\frac{\alpha_4 C_4}{v_e \eta_o}\right)^{1/3}$$

(53)

and

$$\frac{\gamma_4}{\Delta_4} = \pm 1.16 \cdot \frac{I'(\beta) + \left(\frac{2\mu_e Z^2}{\mu_I}\right)^{1/6}}{I''(\beta) + \left(\frac{2\mu_e Z^2}{\mu_I}\right)^{1/6}}$$

For RENT conditions, thermodynamic calculations⁽¹⁷⁾ show that for $p = 80$ atm and $T = 6000$ K (i.e., model gas-cap conditions) the dominant ion is NO^+ since

$$N_{\text{NO}^+} \approx N_e \quad (54)$$

Therefore,

$$Z = 1$$

$$\mu_I = \mu_{\text{NO}^+} = 30.02 \text{ AMU} \quad (55)$$

$$\mu_e = 5.49 \times 10^{-4} \text{ AMU}$$

and

$$\left(\frac{2\mu_e Z^2}{\mu_I}\right)^{1/6} = 0.18 \quad (56)$$

Examination of Equations (53) and (56) indicates that, for the RENT environment, NO^+ ion collisions will increase the total Stark broadening by at least 20 percent. However, the Stark shift will be affected by ion collisions only for low β lines (i.e., $I'' \ll I'$) since the term of Equation (56) appears in both the numerator and denominator of Equation (53). Other ions will not contribute significantly to line broadening in the RENT

environment since their number densities are at least two orders of magnitude less than that of the NO^+ ion. With the above modification, Lindholm's formulation was adopted for the present impact theory analysis. Other, more complex collision theories could be used. However, Lindholm's representation does predict the main features of atomic line broadening and shift without undue mathematical complication. The remaining problem is to specify the constants necessary to calculate line broadening and shift for the RENT flow environment using Lindholm's analytical formulation.

5. Determination of Collision-Broadening Constants

There are specific constants given in Equations (45) and (53) [i.e., α_n , C_n , β , $I'(\beta)$, $I''(\beta)$] which must be determined for each line of interest before collision broadening can be accurately calculated. Some of these constants are available from the literature and others must be estimated. It is the purpose of this section to identify the best available values for these constants in order to compute line broadening in the RENT environment.

Table 1 gives the "best estimate" for values of α_n , η_o , and corresponding ρ_o that are reported by various authors. The term "best estimate" is used here because it is often difficult to determine exactly what an author used due to differences in defining the line width (i.e., full half-width versus half half-widths) and also because of differences in units (i.e., 2π factor involved in converting circular frequency to ordinary frequency). These α_n differences are not really that important since changes in the empirical constant, C_n , which is experimentally determined, will correct for differences in an author's particular choice or definition of α_n and η_o .

The constants for copper lines of interest are determined from measurements of line width and shift at known thermodynamic conditions. However, a problem arises in the fact that little data actually exist for copper line broadening and shift. Furthermore, most of the data that does exist comes from measurements obtained in low pressures (i.e., 1 atm) free-burning arcs⁽¹⁵⁾ where thermodynamic conditions are often not well

TABLE 1
CONSTANTS USED BY VARIOUS AUTHORS TO DETERMINE THE COLLISION RADIUS

REFERENCE	α_n	η_o	$\rho_o, (\text{cm})$
Ovechkin (15)			
n = 6	$3\pi^2/4$	4.0^+	$1.14 (C_6/v)^{1/5}$
n = 4	$\pi/2$	0.65	$1.35 (C_4/v)^{1/3}$
Miyachi (19)			
n = 6	$3\pi^2/4$	0.61	$1.65 (C_6/v)^{1/5}$
n = 4	$\pi/2$	0.65	$1.35 (C_4/v)^{1/3}$

$^+ \frac{4.0}{2\pi} = 0.64$ which implies that Ovechkin's analysis may be in error by a factor of 2π ,

$$\text{therefore, } \rho_o \text{ may be low by a factor } (2\pi)^{1/5} \approx \frac{1.65}{1.14} = \frac{\rho_o (\text{Miyachi})}{\rho_o (\text{Ovechkin})}$$

quantified. AFFDL has sponsored experimental efforts to measure the broadening and shift constants of copper lines in air using a shock tube operating at conditions typical of the RENT flow environment. However, only Van der Waals data (i.e., C_6) for the 5106 Å line have been successfully obtained to date⁽¹⁸⁾. Quantum-mechanical methods have also been used to calculate C_n 's⁽¹⁹⁾. Values of the collision-broadening constants from various sources are given in Table 2. Note that the sign of the C_4 and C_6 constants indicates the direction of shift of the line; i.e., a negative sign implies a red shift. Examination of Table 2 indicates that the majority of information on copper line broadening and shift comes from Ovechkin's data from a free-burning arc. Miyachi's calculations of C_4 for the 5153 Å line disagree with Ovechkin's measurements by a factor of 3. Calspan's C_6 results at elevated pressures (i.e., 90 atm) seem to disagree with Ovechkin's C_6 results but only by a factor of 1.7. However, Ovechkin's formulation for Van der Waals broadening uses a different ρ_0 value than that used to determine C_6 using Calspan's data since the latter used the ρ_0 formulation of Miyachi (see Table 1). Hence, the actual Calspan η_0 , C_6 combination predicts a factor of 2.6 greater line width for Van der Waals broadening than was inferred from Ovechkin's results. A decision is required as to which values given in Table 2 are to be used in the present analysis.

It was decided that Calspan's C_6 value for the 5106 Å line was more representative of broadening conditions in the RENT environment. The value given by Ovechkin for C_6 of the 5153 Å line was then modified to reflect the same order-of-magnitude difference in C_6 as measured by Ovechkin, so that

$$\begin{aligned} C_6(5106) &= -1.7 \times 10^{-32} \\ C_6(5153) &\approx -1.7 \times 10^{-31} \end{aligned} \quad (57)$$

Since no other data are presently available, Ovechkin's values were assumed for the remainder of the constants given in Table 2.

Up to this point, the formulations for collisional line width and shift have been given in circular frequency units. To convert these values to wavelength units in Angstroms, we must use the conversion factor

TABLE 2
BROADENING CONSTANTS REPORTED BY VARIOUS AUTHORS FOR COPPER LINES OF INTEREST

Reference	C_4 (cm^4/sec)	β	$I'(\beta)$	$I''(\beta)$	$\frac{\gamma_4}{\Delta_4}$	C_6 (cm^6/sec)	$\frac{\gamma_6}{\Delta_6}$
<u>Ovechkin</u> ⁽¹⁵⁾							
5106	-1.5×10^{-14}	>1	1.0	1.0	1.16	-1×10^{-32}	2.8
5153	8.1×10^{-14}	.12	1.1	0.47	4	-1×10^{-31}	2.8
<u>Miyachi</u> ⁽¹⁹⁾							
5106	-	-	-	-	-	-	-
5153	2.9×10^{-14}	-	-	-	-	-	-
<u>Calspan</u> ⁽¹⁸⁾							
5106	-	-	-	-	-	-1.7×10^{-32}	2.2
5153	-	-	-	-	-	-	-

$$\gamma, \Delta [\text{\AA}] = \gamma, \Delta [\text{sec}^{-1}] \times \frac{\lambda^2}{2\pi c} \times 10^8$$

where λ is in cm, and c , the velocity of light, is in cm/sec.

In summary, we can write the entire set of equations necessary to compute collisional line broadening using Tables 1 and 2, and Equations (45), (53), and (57) to obtain

$$\gamma_6 = 17.0 c_6^{2/5} v_N^{3/5} N_N \frac{\lambda^2}{2\pi c} \times 10^8 \quad [\text{\AA}]$$

$$\frac{\gamma_6}{\Delta_6} = 2.8$$

$$v_N = \sqrt{\frac{8RT}{\pi} \left(\frac{1}{\mu_{c\alpha}} + \frac{1}{\mu_N} \right)}$$

(58)

$$c_6 = \begin{cases} -1.7 \times 10^{-32}, \lambda = 5105.5 \times 10^{-8} \\ -1.7 \times 10^{-31}, \lambda = 5153.2 \times 10^{-8} \end{cases} [\text{cm}^6/\text{sec}]$$

$$\gamma_4 = 11.4 c_4^{2/3} v_e^{1/3} N_e \left[I'(\beta) + \left(\frac{2\mu_e Z^2}{\mu_I} \right)^{1/6} \right] \frac{\lambda^2}{2\pi c} \times 10^8 [\text{\AA}]$$

$$\frac{\gamma_4}{\Delta_4} = \pm 1.16 \frac{I'(\beta) + (2\mu_e Z^2 / \mu_I)^{1/6}}{I''(\beta) + (2\mu_e Z^2 / \mu_I)^{1/6}}$$

where

λ (cm)	c_4 (cm ⁴ /sec)	$I'(\beta)$	$I''(\beta)$
5105.5 x 10 ⁻⁸	-1.5 x 10 ⁻¹⁴	1.0	1.0
5153.2 x 10 ⁻⁸	8.1 x 10 ⁻¹⁴	1.1	0.47

and

$$v_e = \sqrt{\frac{8RT}{\pi\mu_e}}$$

The above equations can be reduced to simpler forms by substituting appropriate values for the various parameters to obtain

$$\gamma_6 = 5.96 \times 10^{-22} N_N T^{3/10} [\text{\AA}] \quad (5106)$$

$$\gamma_6 = 1.52 \times 10^{-21} N_N T^{3/10} [\text{\AA}] \quad (5153)$$

$$\frac{\gamma_6}{\Delta_6} = 2.8$$

$$\gamma_4 = 9.66 \times 10^{-19} N_e T^{1/6} [\text{\AA}] \quad (5106)$$

$$\gamma_4 = 3.29 \times 10^{-18} N_e T^{1/6} [\text{\AA}] \quad (5153)$$

$$\frac{\gamma_4}{\Delta_4} = -1.16 \quad (5106) \quad (59)$$

$$\frac{\gamma_4}{\Delta_4} = +2.28 \quad (5153)$$

$$\gamma_c = \gamma_6 + \gamma_4$$

$$\Delta_c = \Delta_6 + \Delta_4$$

or

$$\Delta_c = \frac{\gamma_6}{2.8} - \frac{\gamma_4}{1.16} \quad (5106)$$

$$\Delta_c = \frac{\gamma_6}{2.8} + \frac{\gamma_4}{2.28} \quad (5153)$$

Results of calculations using these equations to compute line widths and shifts due to collision effects are shown in Figures 3 and 4. A typical RENT nose-tip pressure of 80 atm was used in the analysis to infer the number density of neutrals, N_N , and electrons, N_e , from equilibrium thermodynamic calculations. Note that for conditions characteristic of the RENT nose-tip environment (i.e., $p = 80$ atm, $T = 6000$ K), Van der Waals broadening and shift dominate the Stark effect for the copper lines of interest.

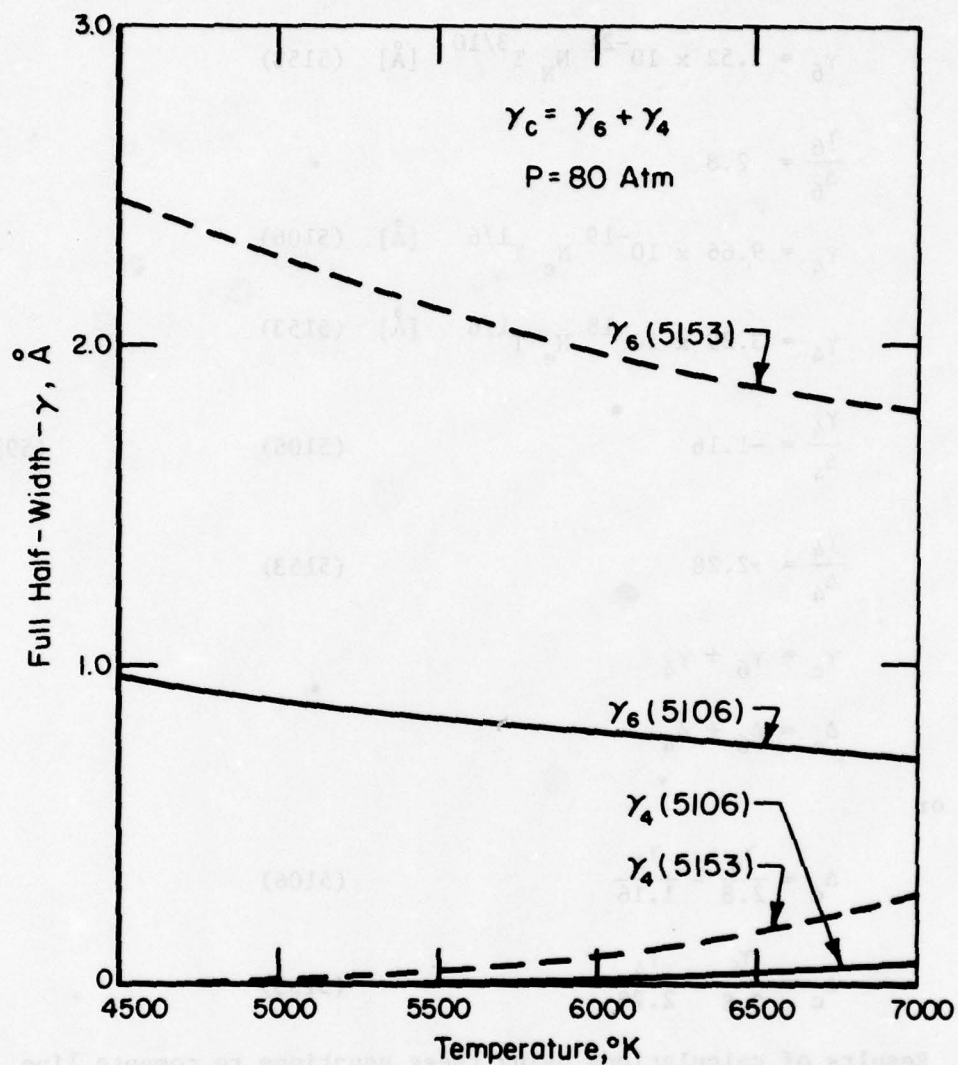


FIGURE 3. COLLISIONAL FULL HALF-WIDTH OF APPROPRIATE COPPER LINES AS A FUNCTION OF GAS TEMPERATURE (p = 80 atm)

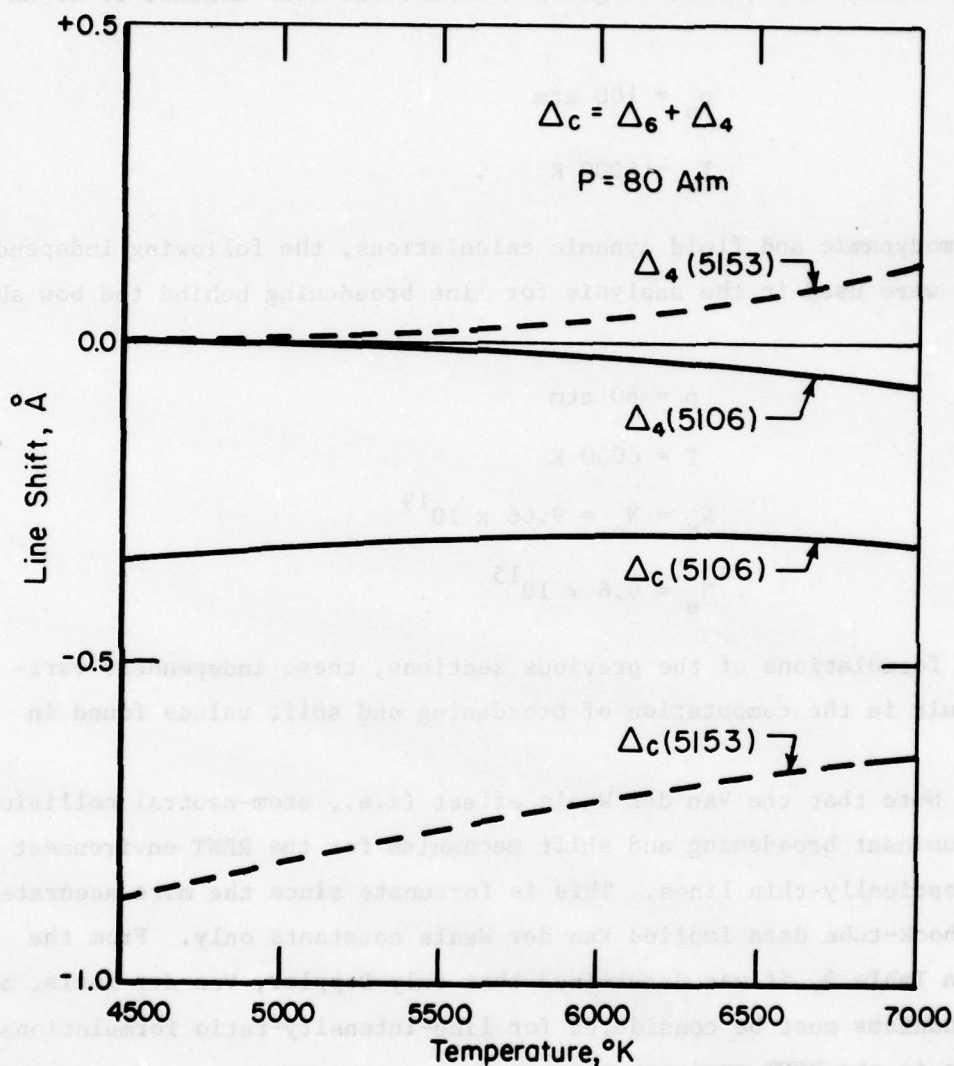


FIGURE 4. LINE SHIFT DUE TO COLLISIONS FOR APPROPRIATE
 COPPER LINES AS A FUNCTION OF GAS
 TEMPERATURE ($p = 80 \text{ atm}$)

F. Summary of Broadening and Shift

In order to identify the important broadening mechanisms in the RENT environment, a calculation was made of the magnitude of various contributions to 5106 and 5153 Å line widths for conditions typical of an arc-tunnel test. The tunnel stagnation conditions were assumed to be as follows:

$$p_o = 100 \text{ atm}$$

$$T_o = 6000 \text{ K} \quad .$$

From thermodynamic and fluid dynamic calculations, the following independent variables were used in the analysis for line broadening behind the bow shock wave:

$$p = 80 \text{ atm}$$

$$T = 6000 \text{ K}$$

$$N_N = N_o = 9.66 \times 10^{19}$$

$$N_e = 6.6 \times 10^{15} \quad .$$

Utilizing formulations of the previous sections, these independent variables result in the computation of broadening and shift values found in Table 3.

Note that the Van der Waals effect (i.e., atom-neutral collisions) was the dominant broadening and shift mechanism for the RENT environment assuming optically-thin lines. This is fortunate since the more accurate Calspan shock-tube data implied Van der Waals constants only. From the results in Table 3, it was determined that only Doppler, Van der Waals, and Stark mechanisms must be considered for line-intensity-ratio formulations applicable in the RENT environment.

If self-absorption is important, the measured line widths, corrected for apparatus function broadening, will be wider than indicated in Table 3. Therefore, the above broadening calculations will be required to determine the unknown copper density from the measured line-width values.

TABLE 3
SUMMARY OF BROADENING AND SHIFT VALUES FOR RENT CONDITIONS

MECHANISM	$\gamma, \text{\AA}$		$\Delta, \text{\AA}$	
	5106	5153	5106	5153
FIXED BROADENING				
Hyperfine Structure	0.04	0.0001	0	0
Isotope Shift	0	0	+0.02	0
Natural Width	0.0001	0.0001	0	0
DOPPLER WIDTH	0.036	0.036	0	0
ZEEMAN BROADENING	0.003	0.003	0	0
COLLISION BROADENING				
Van der Waals	0.784	2.006	-0.28	-0.72*
Stark				
Electron	0.023	0.088	-0.02	+0.04
Ion	0.004	0.015	-0.004	+0.007
Resonance	-	-	0	0

* Note (-) red shift, (+) blue shift

SECTION IV

LINE INTENSITY THEORY

A. General Analytical Form

Use of the simple line-intensity-ratio technique implicitly assumes that the gas under observation emits but does not absorb radiation at the wavelengths of interest (i.e., the gas is optically thin). For the case where this assumption is not valid, a more complex formulation must be developed to correct the measured line-intensity ratio for self-absorption effects. Some of the analytical details required for the above analysis have been reported by Bader^(4,5) but are repeated here for the sake of completeness.

A convenient starting point is the solution to the general equation of radiative transfer of an isothermal slab of gas of thickness ℓ in local thermodynamic equilibrium in which scattering effects and time-dependent effects have been neglected. This solution takes the form⁽²⁰⁾

$$I_{\nu} = B_{\nu}(1 - \exp(-K'_{\nu}\ell)) \quad (60)$$

where

I_{ν} = Observable spectral intensity at frequency ν in units (energy/(time·area·solid angle·frequency))

B_{ν} = Blackbody spectral intensity at frequency ν in units (energy/(time·area·solid angle·frequency))

K'_{ν} = Spectral absorption coefficient including effects of induced emission in units (1/length)

ℓ = Physical thickness of gas slab in units of (length).

The blackbody function, B_{ν} , takes the usual form of

$$B_{\nu} = \frac{2h\nu^3/c^2}{\exp(h\nu/kT) - 1} \quad (61)$$

where

c = Speed of light

h = Planck constant

k = Boltzmann constant

T = Temperature.

The integrated intensity of an isolated spectral line is obtained by integrating Equation (60) over frequency ν , yielding

$$I_{\text{line}} = \int_{\text{line}} I_{\nu} d\nu = \int_{\text{line}} B_{\nu} (1 - \exp(-K'_{\nu} \ell)) d\nu \quad (62)$$

Planck's function, B_{ν} , can be assumed nearly constant for the small frequency extent of the spectral line. This simplifies Equation (62) to yield

$$I_{\text{line}} = B_{\nu_0} \int_{\text{line}} (1 - \exp(-K'_{\nu} \ell)) d\nu \quad (63)$$

where B_{ν_0} is obtained by substituting the line center frequency, ν_0 , into Equation (61).

In order to evaluate the integral in Equation (63), a form for the absorption coefficient, K'_{ν} , must be specified. K'_{ν} is dependent on the broadening mechanism given in Section III. A convenient combination of Doppler and collision-broadening effects (i.e., the dominant broadening mechanisms in the RENT environment) can be modeled into a composite absorption coefficient profile known as a Voigt profile. For this profile, the analytical form of K'_{ν} is given by Penner⁽²¹⁾ as

$$K'_{\nu} = K'_0 H(\alpha, \xi)$$

where

$$H(\alpha, \xi) = \frac{\alpha}{\pi} \int_{-\infty}^{\infty} \frac{\exp(-y^2)}{\alpha^2 + (\xi - y)^2} dy \quad (65)$$

$$K'_0 = \sqrt{\frac{\ell n 2}{\pi}} \frac{1}{1/2 \gamma_D} \int_{\text{line}} K'_{\nu} d\nu \quad (66)$$

$$\alpha = \left(\frac{\gamma_c}{\gamma_D} \right) \sqrt{\ell n 2} \quad (67)$$

and

$$\xi = \frac{(\nu - \nu_0)}{1/2 \gamma_D} \sqrt{\ln 2} \quad (68)$$

Expressions for the collision and Doppler line full half-width (i.e., γ_D and γ_c) are given in Equations (16) and (59), respectively.

The integrated absorption coefficient given in Equation (66) can be related to the atomic transition probability of the line as ⁽²¹⁾

$$\int_{\text{line}} K'_\nu d\nu = \frac{c^2}{8\pi\nu_0^2} A_{uL} \frac{g_u}{g_L} N_L (1 - \exp(-h\nu_0/kT)) \quad (69)$$

Using a Boltzmann distribution to describe the population, N_L , of the electronic energy levels yields

$$N_L = N_u \frac{g_L}{g_u} \exp(E_u - E_L)/kT = N_u \frac{g_L}{g_u} \exp(h\nu_0/kT) \quad (70)$$

where

g_u, g_L = Degeneracy of upper and lower states of the transition

E_u, E_L = Energy of upper and lower energy levels of the transition (Joules)

N_u, N_L = Population of the upper and lower energy levels (cm^{-3})

A_{uL} = Atomic transition probability (sec^{-1})

and the copper atom number density in the upper and lower states can be related to the total number density of copper atoms, $N_{o\text{Cu}}$, using the following:

$$N_u = N_{o\text{Cu}} g_u \frac{\exp(-E_u/kT)}{\sum_i g_i \exp(-E_i/kT)} \quad (71)$$

$$N_L = N_{o\text{Cu}} g_L \frac{\exp(-E_L/kT)}{\sum_i g_i \exp(-E_i/kT)} \quad (72)$$

Hence, substituting Equation (70) and (71) into Equation (69), the integrated absorption coefficient can be written as

$$\int_{\text{line}} K'_v dv = \frac{c^2}{8\pi\nu_o} g_u A_{uL} N_{oCu} \frac{e^{-E_u/kT}}{Q_A} (e^{h\nu_o/kT} - 1) \quad (73)$$

where the atomic partition function, Q_A , is given by

$$Q_A = \sum_i g_i \exp(-E_i/kT) \quad (74)$$

The so-called "Voigt function" (i.e., $H(\alpha, \xi)$) in Equation (65) is not solvable in closed form. However, Armstrong⁽²²⁾ wrote a FORTRAN IV computer code to calculate $H(\alpha, \xi)$ to an accuracy of two digits in the sixth significant figure. The code, as reported in this reference, had several errors which when corrected provided a convenient means of computing the Voigt function for use in determining the copper-line-intensity profiles of interest.

Normalization of the integrated line intensity in Equation (11) by $\gamma_D B_{\nu_o} / \sqrt{\ln 2}$ yields the following:

$$\frac{I_{\text{line}} \sqrt{\ln 2}}{\gamma_D B_{\nu_o}} = \frac{1}{2} \int_{\text{line}} (1 - \exp(-K'_o \ell H(\alpha, \xi))) d\xi \quad (75)$$

The integral in Equation (75) has been numerically computed for various values of $K'_o \ell$ and α . Janson and Korb⁽²³⁾ give this parameter in tabular form to an accuracy of four significant figures. Use of this tabulation results in the determination of integrated line intensities to an accuracy of 0.40 percent by linear interpolation between tabulated values. The table covers a range from weak to fairly strong absorption.

The above set of equations and numerical procedures represent the line-intensity profile shape and the integrated line intensity as a function of pressure, temperature, copper density, and optically-observed path length [i.e., requirements for Equation (4)]. The width of this emission profile can also be determined using the above results. Presently, no closed-form solution is available to represent the line width, γ , as a function of the above dependent variables [i.e., Equation (5) is not

available in explicit form]. However, $\gamma(p, T, N_o, \ell)$ is available implicitly from the above computational procedures. The formulations presented in this section can therefore be used, as discussed in Section I, to correct the measured line-intensity ratio for self-absorption effects.

1. Optically-Thin Limit

For an optically-thin gas, $K'_v \ell$ is much less than one and the exponential term in Equation (60) can be approximated by the first two terms in the series expansion for the exponential, or

$$\exp(-K'_v \ell) \approx 1 - K'_v \ell \quad (76)$$

Substituting Equation (76) into Equation (60) yields

$$I_v = B_v K'_v \ell \quad (77)$$

With this simplification, Equation (63) can also be rewritten as

$$I_{\text{line}} = B_{v_o} \ell \int_{\text{line}} K'_v dv \quad (78)$$

Finally, substituting Equations (73) and (61) into Equation (78), we find that

$$I_{\text{line}} = h\nu_o \frac{g_u A_{uL}}{4\pi} N_o \ell \frac{\exp(-E_L/kT)}{Q_A} \quad (79)$$

For the optically-thin case, Equation (79) shows that the total intensity of any copper emission line is linearly proportional to the product of copper density and optical path length. Therefore, in the ratio of two optically-thin lines, these factors cancel out to produce the following ratio equation using $\nu \propto 1/\lambda$ to obtain

$$\frac{I_1}{I_2} = \frac{\lambda_2}{\lambda_1} \frac{g_{u_1} A_{uL_1}}{g_{u_2} A_{uL_2}} \exp \frac{-(E_{u_1} - E_{u_2})}{kT} \quad (80)$$

where λ_1 and λ_2 are wavelengths of the 5106 and 5153 Å lines, respectively. Solving Equation (80) for temperature yields the desired result

$$T = \frac{\frac{hc}{k} \left(\frac{E_{u_2}}{hc} - \frac{E_{u_1}}{hc} \right)}{\ln \left(\frac{I_1}{I_2} \right) + \ln \left(\frac{\lambda_1}{\lambda_2} \frac{g_{u_2} A_{uL_2}}{g_{u_1} A_{uL_1}} \right)} \quad [K] \quad (81)$$

From review data of Corliss and Bozman⁽²⁴⁾, Table 4 was compiled for use in Equation (81) and Equation (73). Hence, the above equation can be written as

$$T(\text{optically thin}) = \frac{2.756 \times 10^4}{\ln \left(\frac{I_1}{I_2} \right) + 3.425} \quad [K] \quad (82)$$

where

I_1 = Integrated intensity of the 5106 Å line

I_2 = Integrated intensity of the 5153 Å line.

In computing Equation (82), the values of Table 4 were used to obtain a transition probability ratio

$$\frac{g_2 A_2}{g_1 A_1} = 31 \quad (83)$$

Transition probability data obtained by Calspan⁽¹⁸⁾ indicates that

$$\frac{g_2 A_2}{g_1 A_1} = 41 \pm 4 \quad (84)$$

Using the above gA ratios, plots of temperature as a function of measured line intensity ratio for each of the above cases is shown in Figure 5. Note the large dependence of the ratio I_1/I_2 with small changes in temperature for values less than 4000 K. This curve indicates that the region for best application of the 5106/5153 intensity ratio is between 4000 and 8000 K. Also note the importance of having an accurate value for the transition probability ratio of a given line pair. A 7 percent error would have resulted in the measured temperature under optically-thin

TABLE 4
EMISSION CONSTANTS FOR COPPER LINES OF INTEREST

WAVELENGTH λ (Å)	ENERGY LEVELS $\frac{E_i}{hc}$ (cm ⁻¹)		$g_u A_{ul}$ (sec ⁻¹)
	u	l	
5105.541	30783.7	11203.6	0.079×10^{-8}
5153.235	49935.2	30535.3	

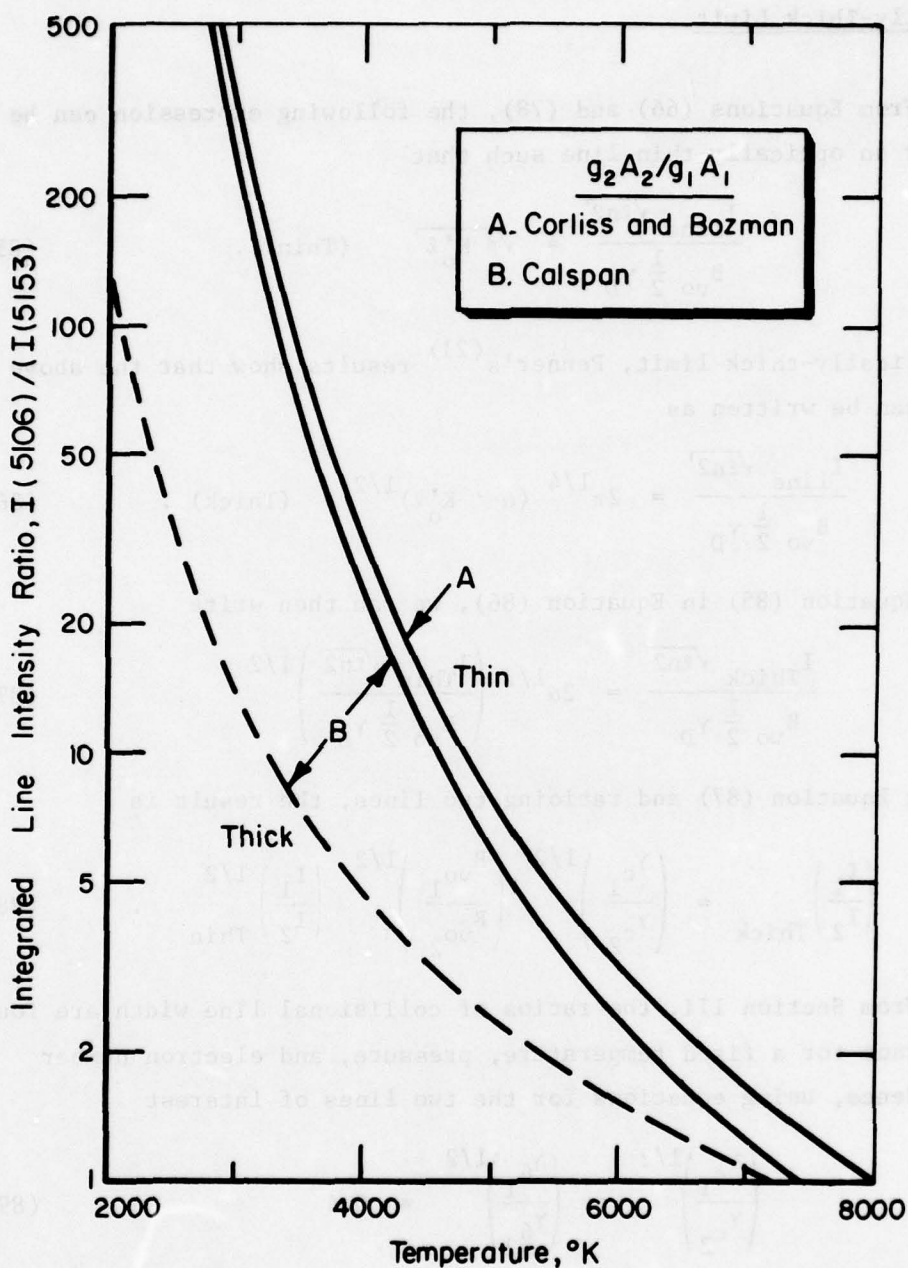


FIGURE 5. INTEGRATED LINE-INTENSITY RATIO AS A FUNCTION OF GAS TEMPERATURE FOR OPTICALLY-THIN AND -THICK LIMITS

conditions if Corliss and Bozman's gA values were utilized near 6000 K instead of Calspan's results.

2. Optically-Thick Limit

From Equations (66) and (78), the following expression can be derived for an optically-thin line such that

$$\frac{I_{\text{line}} \sqrt{\ell n^2}}{B_{\text{vo}} \frac{1}{2} \gamma_D} = \sqrt{\pi K'_O \ell} \quad (\text{Thin}) . \quad (85)$$

For the optically-thick limit, Penner's⁽²¹⁾ results show that the above parameter can be written as

$$\frac{I_{\text{line}} \sqrt{\ell n^2}}{B_{\text{vo}} \frac{1}{2} \gamma_D} = 2\pi^{1/4} (\alpha \cdot K'_O \ell)^{1/2} \quad (\text{Thick}) . \quad (86)$$

Employing Equation (85) in Equation (86), we can then write

$$\frac{I_{\text{Thick}} \sqrt{\ell n^2}}{B_{\text{vo}} \frac{1}{2} \gamma_D} = 2\alpha^{1/2} \left(\frac{I_{\text{Thin}} \sqrt{\ell n^2}}{B_{\text{vo}} \frac{1}{2} \gamma_D} \right)^{1/2} . \quad (87)$$

Simplifying Equation (87) and ratioing two lines, the result is

$$\left(\frac{I_1}{I_2} \right)_{\text{Thick}} = \left(\frac{\gamma_{c1}}{\gamma_{c2}} \right)^{1/2} \left(\frac{B_{\text{vo}1}}{B_{\text{vo}2}} \right)^{1/2} \left(\frac{I_1}{I_2} \right)_{\text{Thin}}^{1/2} . \quad (88)$$

From Section III, the ratios of collisional line width are found to be constant for a fixed temperature, pressure, and electron number density. Hence, using equations for the two lines of interest

$$\left(\frac{\gamma_{c1}}{\gamma_{c2}} \right)^{1/2} \approx \left(\frac{\gamma_{61}}{\gamma_{62}} \right)^{1/2} = 0.4 \quad (89)$$

since Stark broadening is negligible. The ratio of blackbody functions, B_{vo} , for the line is a weak function of temperature only. Hence, for the optically-thick limit, again an expression for the ratio of integrated

line intensities is a function only of the gas temperature (i.e., copper density and path length cancel out). Calculations of the optically-thick line-intensity ratio were performed using equations and constants given in Sections III and IV. The results are also shown plotted in Figure 5 along with the optically-thin computations. Note that significant temperature error could result if measurements of optically-thick lines are used in conjunction with optically-thin theory. The opposite is also true; therefore, the copper density must be known or large errors are possible utilizing the line-ratio method.

SECTION V

DESCRIPTION OF COMPUTATIONAL PROCEDURES

Analytical formulations for computing the line intensity profiles of the 5106 and 5153 Å copper lines which are given in Sections III and IV were coded into a FORTRAN IV digital computer program. For a detailed description of this program, the reader should consult Reference 25.

The input variables required by the code are as follows:

Gas pressure, p , in atm

Gas temperature, T , in °K

Optical path length, l , in cm

Copper number density, N_{Cu} , in atoms/cm³

Various atomic constants.

The code first calculates the true line shape (i.e., infinitely-narrow instrument apparatus function) using Equations (60), (61), (64) through (68), and (73). The results of this calculation are plotted along with a printout of the ratio of line peak intensities, the integrated line-intensity ratio, and the ratio of the widths of the two lines (i.e., γ_1/γ_2). A table look-up routine is supplied for the thermodynamic calculations to provide values for the number density of neutrals and electrons given the temperature and pressure. The table was constructed using data provided in Neel's computations⁽²⁶⁾. Table look-up results are also printed out as part of the code output. The partition function, Q_A , is also provided as a table look-up based on calculations using Equation (74).

Computation of true line shape is accomplished by calculating the "Voigt function" using Armstrong's numerical methods⁽²²⁾ for wavelength positions from the line center to a wavelength where the intensity was less than 0.1 percent of the peak intensity value. This line contour is then numerically analyzed to determine the peak intensity and the full half-width of the line. The profile was also numerically integrated using Simpson's rule to obtain the integrated line intensity value. These true line-shape results are printed out along with the input parameters for the particular calculations.

Since most spectral data are obtained with a finite apparatus function width, some convolution occurs and the true line shape is altered

due to the shape of the apparatus function. Therefore, the code also included a convoluting routine to convert the above true line contour into the profile actually measured by the spectroscopic equipment. The apparatus function used to perform this convolution was assumed to be Gaussian in nature. Hence, the function was completely defined for a given full half-width of the Gaussian line profile which is the final input parameter. This apparatus function width, γ_A , was determined from experimental data obtained using an infinitely-thin calibration line from standard sources (i.e., copper hollow-cathode lamp). A provision was also incorporated into the code to allow separate apparatus functions for each of the two lines of interest (i.e., γ_{A1} and γ_{A2}). Other apparatus function shapes could be coded if necessary. Once the convolution calculation was performed, the convoluted profile was also numerically analyzed to provide peak intensity ratios, integrated intensity ratios, and apparent line widths for actual measurement conditions. These results were also printed as part of the code output. Measured spectral data could then be compared directly with theoretical values to avoid the necessity for deconvolution of the measured line-intensity profile data.

Several other parameters are printed out for each line of interest. They are as follows:

K'_0, α - From Equations (66) and (67), respectively

B_{v_0} - Equation (61)

I^P - Peak line intensity

I_{line} - Integrated line intensity

γ - Actual full half-width of the line in Å

$\gamma_D, \gamma_4, \gamma_6$ - Doppler, Stark, and Van der Waals contributions to the true width, in Å.

The above code output completely defines the shape of and intensity parameters for the 5106 and 5153 Å lines. Pressure, optical path length, and apparatus function widths are usually held constant while temperature and copper density are varied to generate a matrix of dependent variables using the above code. Plots of these dependent parameters as a function of

temperature and copper density can be used to reduce spectroscopic data from the arc-tunnel flow in order to obtain the gas flow static temperature and unknown copper density corrected for self-absorption effects on the emission spectra.

Apparatus function used to perform this correction is defined for a Gaussian in nature. Hence, the function was completely defined for a given full width of the Gaussian line profile which is the final input parameter. This apparatus function with γ was determined from experimental data obtained using an initially thin calibration line from standard sources (i.e., copper I (low-energy) lamp). A provision was also incorporated into the code to allow separate apparatus functions for each of the lines of interest (i.e., γ_{Cu} and γ_{Ar}). Other apparatus functions shapes could be coded if necessary. Once the convolution calculation was performed, the convolved profile was also numerically analyzed to provide peak intensity ratios, integrated intensity ratios, and apparent line widths for actual measurement conditions. These results were also printed as part of the code output. Measured spectral data could then be compared directly with theoretical values to avoid the necessity for deconvolution of the measured line-intensity profile data.

Several other parameters are printed out for each line of

interest. They are as follows:

K'_{Cu} , K'_{Ar} - from Equations (6a) and (6b), respectively

K_{Cu} , K_{Ar} - Equation (6c)

I_p - Peak line intensity

I_{int} - Integrated line intensity

γ - Actual full width of the line in Å

γ_{Cu} , γ_{Ar} - Doppler, Stark, and Van der Waals contributions to the line width, in Å

The above code output completely defines the shape of and intensity parameters for the 5105 and 5153 Å lines. Pressure, optical path length, and apparatus function widths are usually held constant while temperature and copper density are varied to generate a matrix of dependent variables using the above code. Most of these dependent parameters are a function of

SECTION VI

DISCUSSION OF ANALYTICAL RESULTS

The computer code described briefly in Section V was exercised for the following input conditions:

$$\begin{aligned}p &= 80 \text{ atm} \\ \ell &= 2 \text{ cm} \\ \gamma_{A1} &= 1.64 \text{ \AA} \\ \gamma_{A2} &= 1.41 \text{ \AA} \\ T &= 4500\text{--}8000 \text{ K in } 500 \text{ K increments} \\ N_{\text{Cu}} &= 10^{14}, 10^{15}, 2 \times 10^{15}, 5 \times 10^{15}, 10^{16}, 2 \times 10^{16}, \\ &\quad 5 \times 10^{16} \text{ atoms/cm}^3.\end{aligned}$$

It should be noted that the present choice of apparatus function widths was not fortuitous, but represents values obtained in later experimental work by the present author. The two functions had different half-widths due to the slight difference in the focal properties of the measurement instrument. These apparatus function widths also are representative of values used by Bader⁽⁶⁾ in a four-channel polychromater instrument which employed a trapezoidal apparatus function that had a full half-width of 1.79 Å and a base width of 2.66 Å. Therefore, the observations stated below have validity for both past and present experimental efforts. Results of theoretical computations for true line contours (i.e., $\gamma_A = 0$) and relative line intensities are shown in Figure 6 for $T = 6000 \text{ K}$ as a function of flow copper density. In Figure 7, the same results are shown for both lines but, in this case, the true line contours have been convoluted with the proper full half-width, Gaussian-shaped apparatus functions to indicate measured line profile conditions.

Note that at fixed temperature and pressure (i.e., constant collisional and Doppler broadening), the following effects occur for each of the lines as the copper density increases.

- Line full half-width increases due to self-absorption effects near the center of each line.

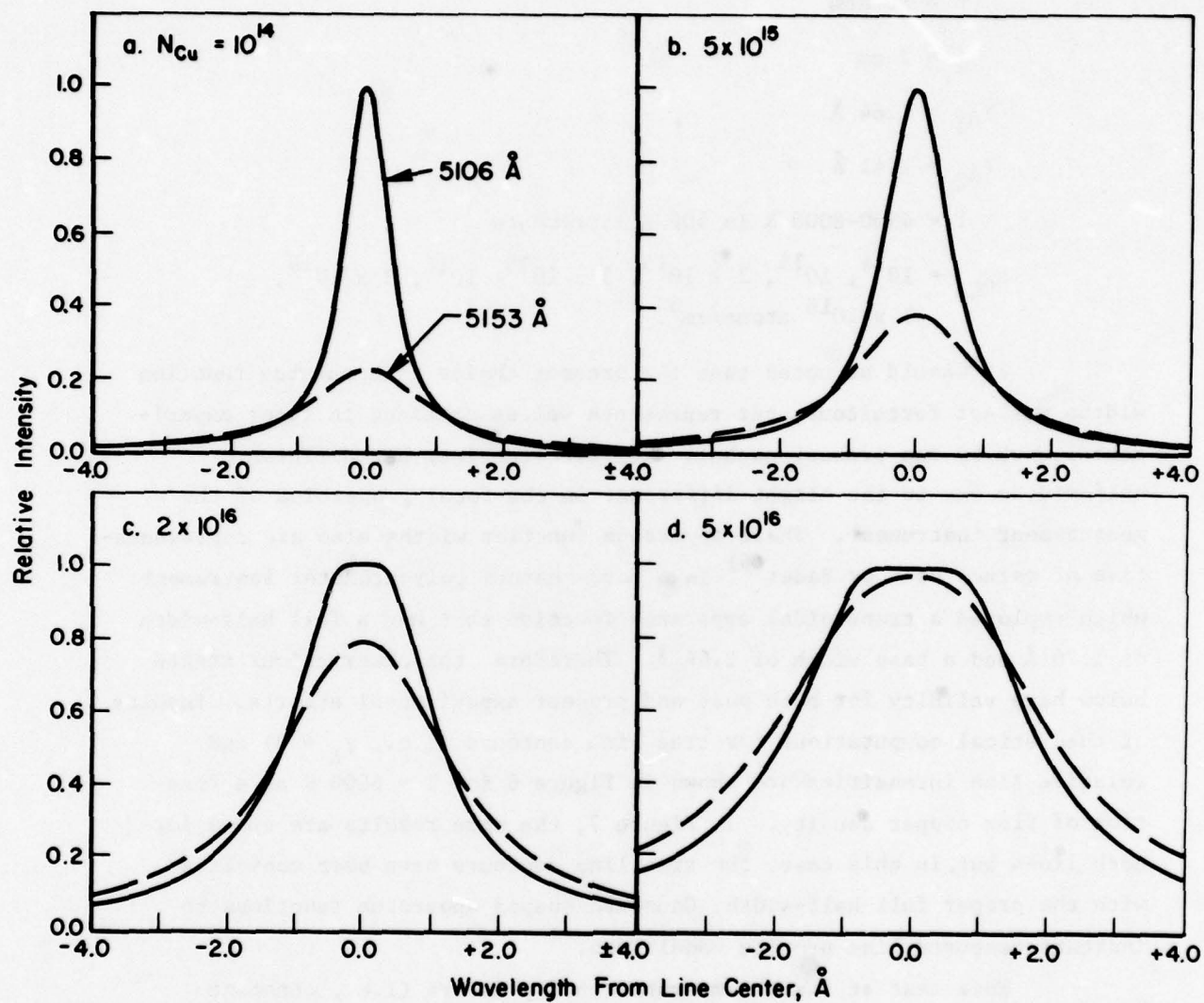


FIGURE 6. TRUE LINE CONTOUR AND RELATIVE LINE INTENSITY CHANGES WITH INCREASING COPPER NUMBER DENSITY ($p = 80$ atm, $l = 2$ cm, $\gamma_A = 0$)

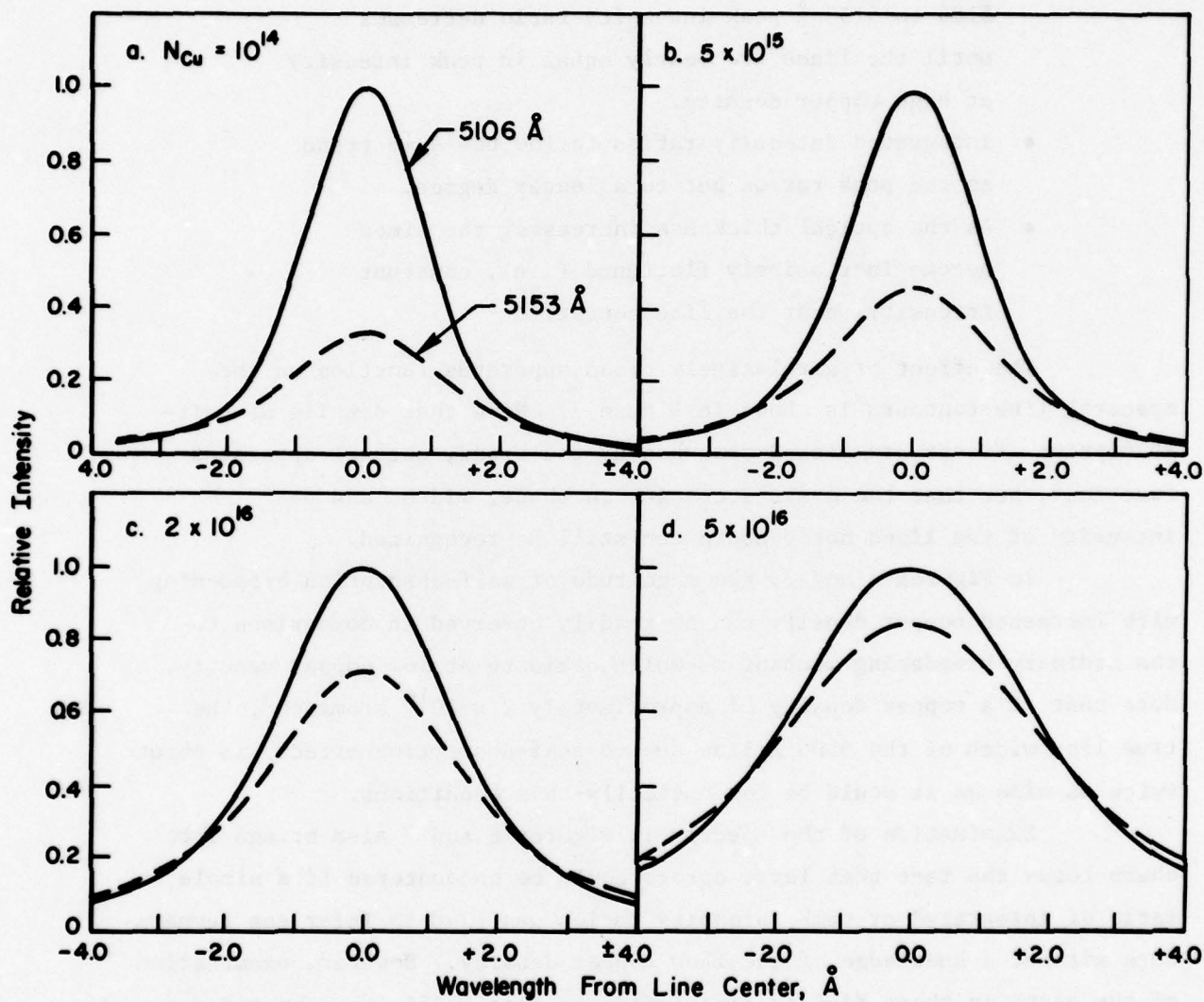


FIGURE 7. MEASURED LINE CONTOUR AND RELATIVE LINE INTENSITY CHANGES WITH INCREASING COPPER NUMBER DENSITY ($p = 80$ atm, $l = 2$ cm, $\gamma_{A_1} = 1.64$ Å, $\gamma_{A_2} = 1.41$ Å)

- The width of the 5106 Å line is less than the 5153 Å line at optically-thin conditions but the width of the former line increases faster with increasing copper density until the two lines are nearly of equal width at high copper density.
- Relative line intensity changes such that the 5106 to 5153 Å peak intensity ratio decreases until the lines are nearly equal in peak intensity at high copper density.
- Integrated intensity ratios follow the same trend as the peak ratios but to a lesser degree.
- As the optical thickness increases, the lines become increasingly flattened (i.e., constant intensity) near the line center.

The effect of a relatively broad apparatus function on the spectral line contours is shown in Figure 7. Note that details of self-absorption effects are masked somewhat by the broad, unequal apparatus functions, but that the overall changes in shape, width, and peak intensity of the lines noted above can still be recognized.

In Figures 6 and 7, the magnitude of self-absorption broadening with increased copper density can be readily observed in comparison to the ordinary broadening mechanisms which dominate at low copper density. Note that at a copper density of approximately 2×10^{16} atoms/cm³, the true line width of the 5106 Å line due to self-absorption effects is about twice as wide as it would be for optically-thin conditions.

Examination of the spectra in Figures 6 and 7 also brings into sharp focus the fact that large errors could be encountered if a simple ratio of integrated or peak intensity ratios was used to infer gas temperature without a knowledge of the flow copper density. However, examination of the plots in these figures also indicates that sufficient changes occur in the line profile shape and full half-width as copper density increases to imply that both copper density and temperature could be simultaneously determined from a measurement of the entire line intensity profile (i.e., peak intensity and line full half-width).

To accomplish this simultaneous temperature/copper density measurement, it is necessary to first compute line peak intensity ratio and line full half-width, for a series of possible copper density/temperature combinations. Results of these computations are shown in Figures 8 and 9 for an infinitely-thin apparatus function as well as one which represents a more realistic set of instrument full half-widths (i.e., $\gamma_{A1} = 1.64 \text{ \AA}$, $\gamma_{A2} = 1.41 \text{ \AA}$).

The particular values of plotting parameters shown in Figures 8 and 9 were chosen for several reasons. Peak intensity ratios were utilized rather than integrated ratio values in order to simplify the data reduction procedure. Absolute magnitude of the 5106 \AA line width was utilized rather than a ratio of the two line widths since Calspan data determined the broadening constants for the 5106 \AA line only.

The curves in Figure 9 could be utilized directly to reduce spectroscopic data taken with the same apparatus function. However, a cumbersome iteration process would be required whereby measured values of intensity ratio and 5106 \AA line width are used to locate a set of temperature and copper density values that are consistent with both of the measured parameters. A simpler way to reduce the data can be obtained if cross-plots are constructed from the theory plots in Figure 9. These cross-plots are obtained by picking constant values of intensity ratio and line width and finding the points of intersection of these values with the constant temperature and copper density curves in Figure 9. New curves can then be constructed with temperature and density for the variables as shown in Figure 10.

Again in Figure 10, the importance of knowing the copper density is evident in order to infer temperature from line-intensity ratio data. Note that only for narrow (i.e., optically-thin) lines is the line ratio independent of flow copper density.

Comparison of Figures 8 and 9 also indicates that a greater accuracy would be obtainable for this data reduction process if the plots in Figure 10 were constructed with calculations using a narrow apparatus function (i.e., $\gamma_A \ll 1.5 \text{ \AA}$). This is especially true for the line width data because at moderate copper densities the spread between the constant temperature lines is significantly greater for $\gamma_A = 0$ than for $\gamma_A \approx 1.5 \text{ \AA}$. However, for high copper densities (i.e., broad true line widths), even the broader apparatus function is quite acceptable.

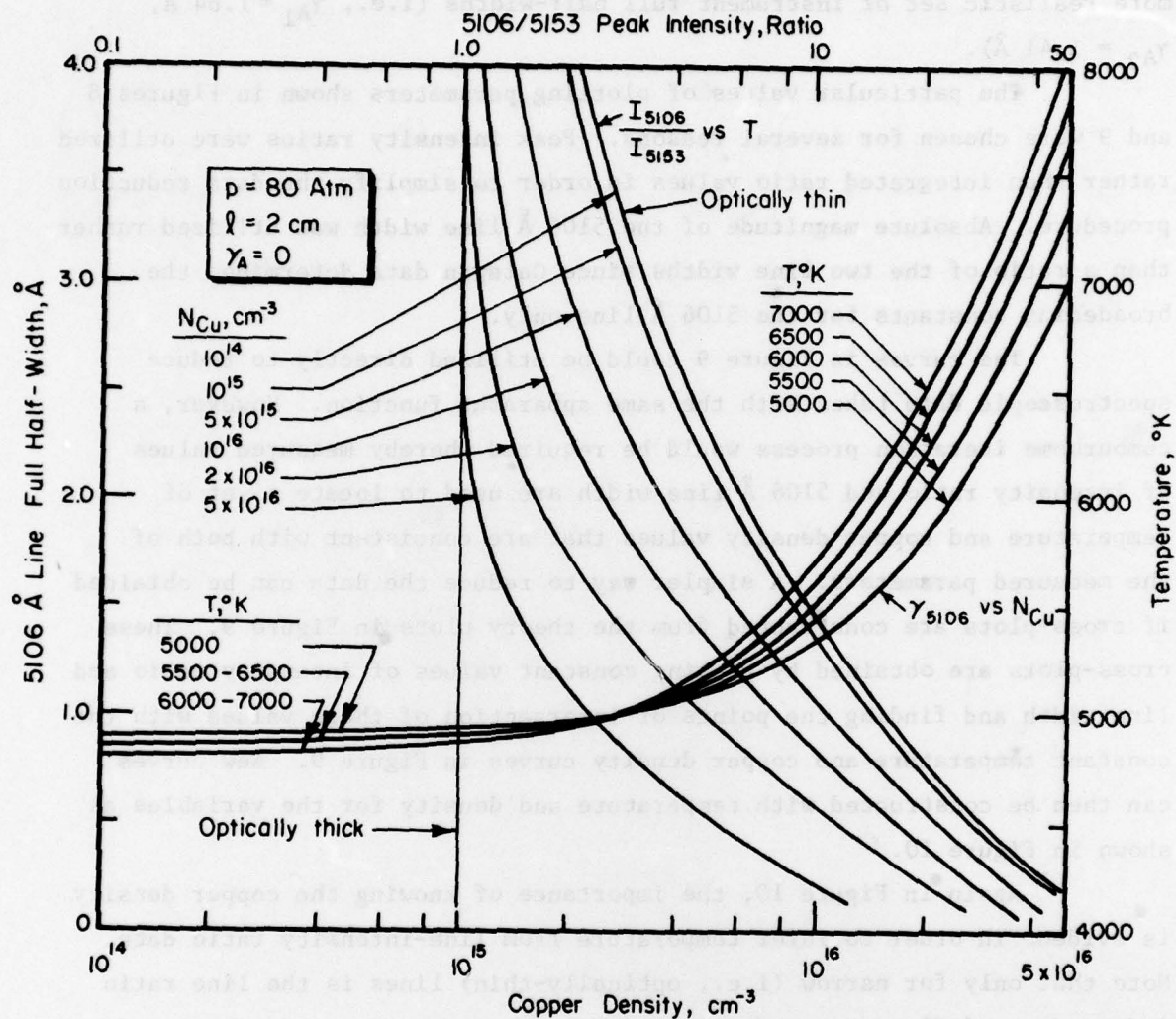


FIGURE 8. RATIO OF LINE PEAK INTENSITIES AND FULL HALF-WIDTH OF THE 5106 Å LINE AS A FUNCTION OF GAS TEMPERATURE AND COPPER DENSITY FOR THE TRUE LINE SHAPES

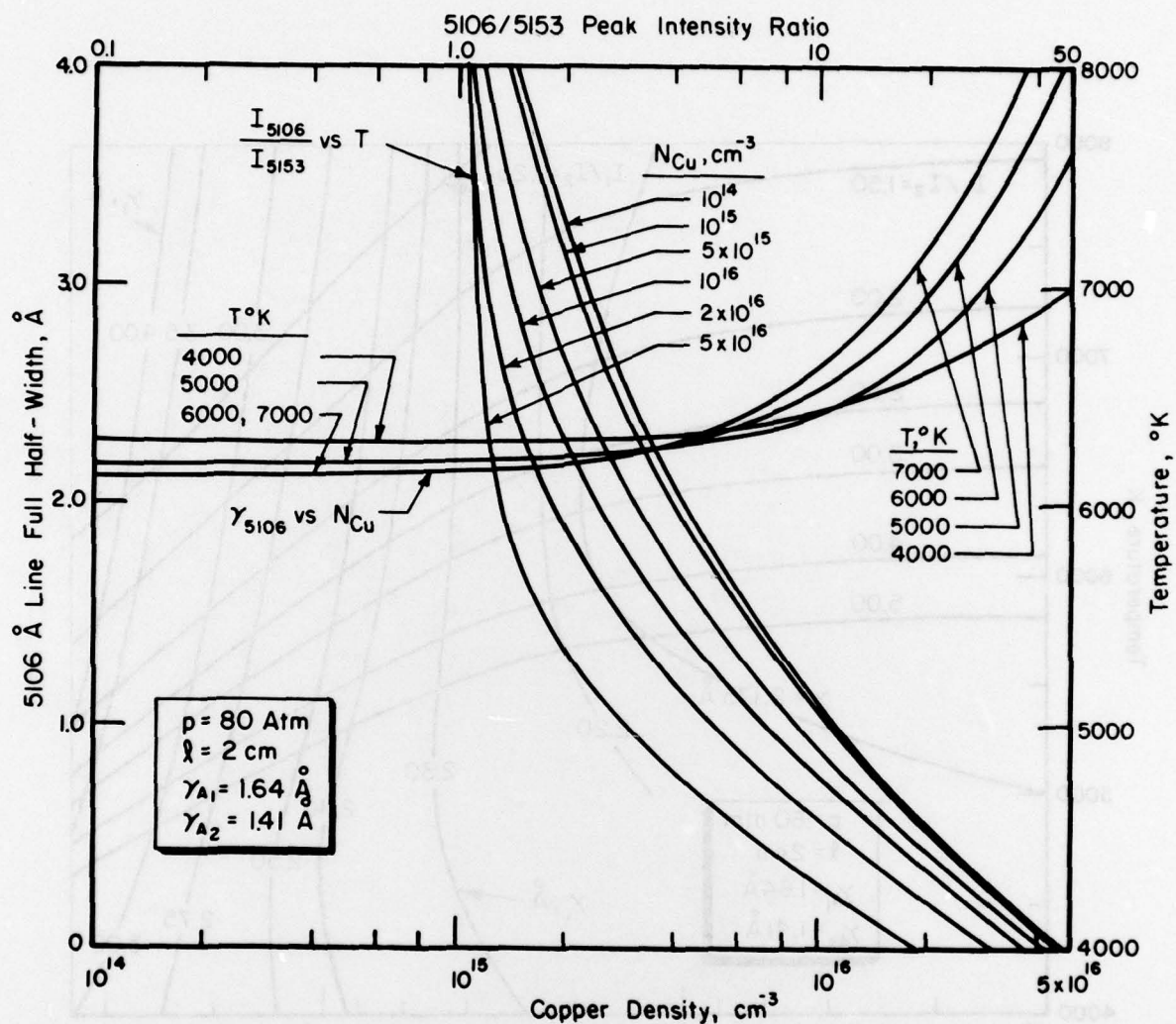


FIGURE 9. RATIO OF LINE PEAK INTENSITIES AND FULL HALF-WIDTH OF THE 5106 Å LINE AS A FUNCTION OF GAS TEMPERATURE AND COPPER DENSITY FOR ACTUAL EXPERIMENTAL CONDITIONS

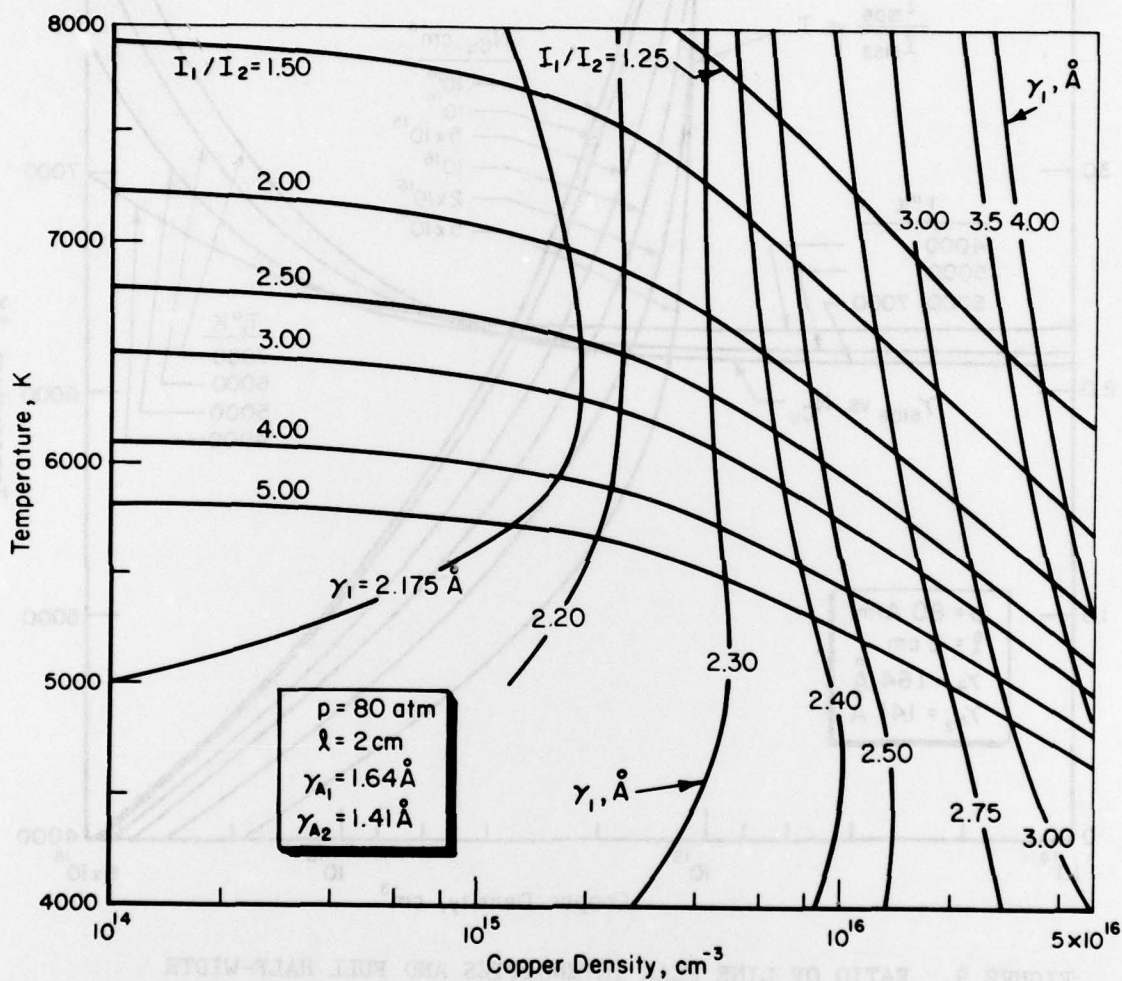


FIGURE 10. DATA REDUCTION PLOTS USED TO DETERMINE COPPER DENSITY AND GAS TEMPERATURE FROM THE MEASURED COPPER LINE SPECTRA

In Figure 10, the intersection of the two families of curves defines compatible temperature/copper density combinations (i.e., solutions to the desired data reduction process). Hence, Figure 10 can be used to quickly determine which temperature and copper density combination that best agrees theoretically with the measured parameters. The process of reducing the data is as follows:

- (1) The curve which most closely represents the measured 5106 Å line width, γ_1 , is first located in Figure 10 using linear interpolation, if necessary.
- (2) The corresponding curve representing the measured peak intensity ratio (I_1/I_2) is then located as above.
- (3) The intersection of these two curves gives the required copper density and temperature.

A more accurate method of analysis would involve construction of curves such as those in Figure 10 for many more constant width and intensity ratio values. Note also that the above data reduction procedure could be easily mechanized and coded into a computer program to automate the data reduction process. This automation was accomplished in the present study and the code was available for computer data reduction.

SECTION VII

ERROR ESTIMATE

The text of this report contains a method to correct the simple line-intensity ratio temperature-measurement technique for self-absorption effects. However, a discussion of this correction method would not be complete without some indication as to the accuracy of the correction procedure. First of all, it is necessary to point out that several other assumptions must be valid before the line-ratio method will provide the most accurate results possible even for optically-thin conditions. These assumptions are

- The temperature, pressure, and copper density are assumed to be spatially uniform over the emission region; that is, the above properties must be spatially homogeneous over the optical path length.
- A corollary to the above assumption is required when radiation from a model nose tip is being examined to infer model stagnation temperature. This corollary states that the free-stream must emit and absorb a negligible amount of radiation compared to these effects in the nose-tip region.

Further, it is assumed that

- Local thermodynamic equilibrium (LTE) exists such that population of the electronic mode of copper is represented by a Boltzmann distribution described by some temperature, T_{Cu}^{el} , that is equal to the static temperature of the gas (i.e., $T_{Cu}^{el} = T$).
- The final assumption is that the measurement time is short compared with any temporal fluctuations in flow properties.

We will presume that the above assumptions are correct such that the only error source is considered to be due to self-absorption effects. The question then is, "How accurate is the self-absorption correction procedure?"

Several dominant sources can be listed as possible causes of error in the self-absorption analysis procedure, and they can be grouped into three categories:

- Measurement inaccuracies
- Erroneous thermodynamic assumptions
- Faulty analytical assumptions.

Measurement inaccuracies are always possible and involve the inability to determine the exact value of the experimental line width and intensity ratio. Without valid measurement values in the first place, it is impossible to accurately correct for self-absorption errors. Another measurement error source is the determination of an exact apparatus function and its associated Gaussian full half-width. Also an accurate value for the optical path length, l , must be obtained from photographic observation of the radiating gas. Finally, the accuracy of measurements made by other experimenters can lead to errors in the present analysis since atomic constants (i.e., $g_1 A_1 / g_2 A_2$, C_6 's) determined by other authors are used in the present correction procedure.

Regarding the thermodynamic assumptions used in the data reduction procedure, it should be noted that the gas pressure is assumed to be known from flow measurements obtained by AFFDL personnel. The pressure is also assumed to be constant over the entire wind-tunnel run. Further, it is assumed that the gas is in chemical equilibrium such that the number density of neutrals and electrons, which are used in the line-broadening calculations, can be determined from the known pressure and the assumed temperature.

The final error category is the inaccuracy of theoretical models used to predict the line shape and intensity. It is felt that the "Voigt" line profile is quite accurate and that Doppler broadening is well understood. On the other hand, the Lindholm theory for collision broadening may not be a true representation of broadening at the high pressure encountered in the RENT arc-heated flow. However, it is difficult to assign an error value to this type of possible inaccuracy because there is presently no exact theory to compare with the Lindholm computational results. Perhaps the line shift information obtained in the RENT environment will sufficiently

corroborate the application of Lindholm's model to the arc-heated flow environment. The theory as coded does predict the width and intensity ratio that were measured by Calspan in shock-tube experiments. These latter measurements were made at conditions similar to the RENT environment so, in actuality, the subtraction of the optically-thin line width from the measured line width to infer copper density tends to be empirically correct.

The accuracy of this self-absorption correction procedure was determined by varying the parameters whose values cannot be specified with certainty by a fixed amount about some base value. Plots such as those in Figure 10 could have been constructed for each parameter variation and the corresponding variation in corrected temperature could be noted. This tedious but straightforward procedure provides an indication of the sensitivity of the inferred temperature to inaccuracies in the above data reduction parameters. Then, an estimate could be made of the possible inaccuracy in these parameters for the actual conditions encountered in a given experiment. Finally, the results from the sensitivity data could then be coupled to the above error estimates to compute a possible error in the corrected temperature based on all the possible inaccuracies in the data reduction parameters.

Actually, this process should have been repeated for each experimental data point because the resulting temperature correction error would vary with the particular region of Figure 10 where the data fell. However, a representative error was obtained by examining a data point that falls nearest the average temperature and copper density values. The baseline intensity ratio of 1.65 and the 5106 line width of 2.69 Å were taken from actual arc-tunnel data that represented a temperature and copper density near the average for all the data obtained (i.e., $T_{\text{baseline}} = 6538 \text{ K}$ and $(N_{\text{Cu}})_{\text{baseline}} = 1.10 \times 10^{16} \text{ atoms/cm}^3$).

The above error estimate process was then undertaken using parameters employed to produce Figure 10 as the baseline case. Each important parameter was then varied about this baseline by a prescribed amount and the corresponding temperature variation was calculated. Some of the analytical parameters have a small effect on the computations so they were left out of the analysis. The computer program written to

automatically perform the required iterations was utilized such that no interpolation or replotting process was necessary. This scheme provided more accurate sensitivity estimates.

Results of this error analysis are shown in Table 5. For each selected variation, ΔPar , in the baseline parameter, a corresponding inferred temperature variation, ΔT , was computed. Therefore, a sensitivity parameter, S , can be computed where

$$S = \frac{\Delta T / T_B}{\Delta \text{Par} / \text{Par}_B} = \frac{\text{Error in Temperature}}{\text{Error in Parameter}} \quad (90)$$

This parameter, S , represents the sensitivity of the inferred temperature to errors or uncertainties in the value of a given parameter. Hence, large sensitivities coupled with large parameter uncertainties result in large measurement errors. The results in Table 5 indicate that the sensitivity is small for all the parameters of interest.

Also given in Table 5 is an estimate of the actual uncertainty in a given parameter, ϵ_{par} . These estimates represent conservative values from the author's own data as well as that of other authors. A value of 50 percent accuracy of C_6 for the 5153 line was based on the fact that no line width measurements were made for this line but the measurements for the other line were within this amount of error from the theoretical values.

Using these error estimates, the actual temperature error, ϵ_T , for each of these error sources could be computed using

$$\text{Temperature Error} \equiv \epsilon_T = S \cdot \epsilon_{\text{par}} \quad (91)$$

These errors are also shown in Table 5 and most are less than 1 percent. The largest error source is due to the uncertainty in the ratio of gA factors for the two lines. Uncertainty in C_6 's is also important. The total possible error equals 13.5 percent (i.e., ± 7 percent), which is a simple sum of all the error sources in Table 5. Therefore, we can write that the measured stagnation temperature, T_0 , is given by

$$T_0 = 6538 \pm 458 \text{ K} \quad (92)$$

The resultant inferred enthalpy error is larger because the sensitivity of enthalpy change to temperature change is greater than one. Hence, the measured stagnation enthalpy was

TABLE 5

ERROR ANALYSIS FOR SELF-ABSORPTION CORRECTION

BASELINE PARAMETER (Par)*	SELECTED VARIATION IN PARAMETER ΔPar	CORRESPONDING TEMPERATURE VARIATION $\Delta T (^{\circ}\text{K})$	SENSITIVITY $S = \frac{\Delta T/T_B}{\Delta \text{Par}/\text{Par}}$	ESTIMATED PARAMETER ERROR, % ϵ_p	TEMPERATURE ERROR $S \times \epsilon_p = \epsilon_T$
$\left(\frac{1}{12}\right)_{\text{meas}} = 1.65$	0.30	377	0.32	3.5%	1.1%
$(\gamma_1)_{\text{meas}} = 2.69 \text{ \AA}$	0.40	369	0.38	3%	1.1%
$(\gamma_A)_1_{\text{meas}} = 1.64 \text{ \AA}$	0.20	265	0.33	3%	1.0%
$(\gamma_A)_2_{\text{meas}} = 1.41 \text{ \AA}$	0.20	223	0.24	3%	0.7%
$\left(\frac{g_2 A_2}{g_1 A_1}\right)_{\text{meas}} = 41$	8	216	0.17	20%	3.4%
$c_6 (5106)_{\text{meas}} = -1.7 \times 10^{-32} \text{ cm}^6/\text{sec}$	-1×10^{-32}	154	0.04	30%	1.2%
$c_6 (5153)_{\text{theor}} = -1.7 \times 10^{-31} \text{ cm}^6/\text{sec}$	-1×10^{-31}	192	0.05	50%	2.5%
$P = 80 \text{ atm}$	10	141	0.17	10%	1.7%
$\lambda = 2 \text{ cm}$	1	124	0.04	20%	0.8%
TOTAL					$\Sigma = 13.5\%$

* Baseline Conditions: $T_B = 6538^{\circ}\text{K}$, $N_{\text{cub}} = 1.10 \times 10^{16} \text{ Atoms/cm}^3$

$$H_o = 5400 \pm 625 \text{ [Btu/lb}_m\text{]}$$

(93)

or the error is ± 12 percent for self-absorption effects only. This enthalpy measurement error could be reduced to less than ± 10 percent by judicious reduction of certain error sources listed in Table 5, especially those relating to uncertainties in the atomic constants.

SECTION VIII

SUMMARY AND CONCLUSIONS

The text of this report contains detailed analytical formulae and appropriate empirical constants required to predict shape and intensity of the copper emission spectrum from a high-temperature, high-pressure plasma including self-absorption effects. In particular, the spectrum of the 5106 and 5153 Å copper lines was calculated for conditions typical of the gas flow environment in the Reentry Nose-Tip (RENT) Facility at the Air Force Flight Dynamics Laboratory (AFFDL). In previous work at AFFDL, a simple intensity ratio from the above lines was used to infer gas temperature in the RENT facility. However, the arc-heated flow contains an unknown amount of copper contaminant, so the above theoretical formulation was required in order to provide a method of correcting the simple line ratio measurement for self-absorption effects.

Development of the analytical expressions presented in this report includes a discussion of various line-broadening mechanisms and an estimate of the relative magnitude of each of the various operative broadening effects. The empirical constants required to predict collisional line broadening of the 5106 Å line for optically-thin conditions were derived from spectral data measured by Calspan under a contract to AFFDL. Data required to compute the magnitude of other broadening effects were not provided by this source and had to be obtained from other references in the open literature.

Based on these calculations, it was found that the dominant broadening mechanisms in the RENT environment included

- Self-absorption broadening due to excessive amounts of copper contaminant
- Van der Waals broadening due to collisions between emitting atoms and neutral particles.

Other less important broadening phenomena that were included for completeness were Doppler and Stark broadening effects. All other broadening mechanisms were found to be negligible for RENT flow conditions (i.e., pressure = 100 atm, temperature ≈ 6000 K, copper density $\approx 10^{16}$ atoms/cm³).

Dominance of collisional broadening mechanisms leads to the use of a "Voigt" line contour shape. This line profile was used to predict the line width and peak line-intensity ratio, as well as, integrated line-intensity ratio as a function of flow copper density, gas pressure, optical path length, and gas temperature. Standard line intensity theory described by Penner was used in these computations with transition probability data also determined by Calspan.

Results of these line shape and intensity ratio calculations showed that, for conditions typical of the RENT flow environment, self-absorption of copper line radiation was significant such that a large error in measured temperature would be encountered if the simple line-intensity ratio was not corrected for self-absorption effects. It was also shown that correction of the simple line-ratio method was indeed possible if a simultaneous measurement was made of the full half-width of the 5106 Å copper line. These two measurements were shown to provide the tedious, but necessary, means to correct the simple line-ratio method such that a more accurate temperature could be inferred from spectroscopic emission data. The present estimate of the temperature error resulting from uncertainties in this self-absorption correction procedure is ± 7 percent for typical RENT peaked-profile stagnation flow conditions. This corresponds to a ± 12 percent error in the enthalpy inferred from the self-absorbed copper line spectral data. This self-absorption correction error could be reduced if more accurate atomic constants were available. Other error sources also need to be examined before a final error estimate can be assigned to the copper-line-ratio techniques for measuring enthalpy in an arc-heated flow.

REFERENCES

- (1) VanKuren, J. T., "An Experimental and Theoretical Investigation of the Nozzle Flow in a Large Arc Heated Hypersonic Wind Tunnel," PhD Dissertation, Ohio State University, 1969.
- (2) Mastrup, F. N., "Development of Spectroscopic and Optical Scattering Diagnostics for Non-Equilibrium Reacting Gas Flows," AFFDL-TR-70-17 (1970).
- (3) Lawrence, L. R., Jr., Walterick, R. E., Weeks, T. M., and Doyle, J. P., Jr., "Total Enthalpy Measurement from Blunt Body Gas-Cap Emission in Arc-Heated Wind Tunnels: Results and Applications," AFFDL-TM-72-22 FX (1972); also AIAA Paper No. 72-1021 presented at AIAA 7th Aerodynamic Testing Conference, Palo Alto, California (September, 1972).
- (4) Baust, H. D., Bader, J. B., "Development of an Electronics Package for Use in Real Time, Optically-Thin, Isothermal Spectral Line Intensity Ratio Temperature Measurements," AFFDL-TR-74-153 (1974).
- (5) Bader, J. B., "Time Resolved Absolute Intensity Measurements of the 5106 Å Copper Atomic Spectral Line in the AFFDL RENT Facility," AFFDL-TR-75-33 (1975).
- (6) Bader, J. B., Unpublished work at the Air Force Flight Dynamics Laboratory.
- (7) Boiarski, A. A., "Detailed Measurements of Line Shape, Line Shift, and Self-Absorption Effects on Stagnation Enthalpy Measurements Using the Copper-Line-Intensity-Ratio Technique," AFFDL-TM-78-33-FXN (1978).
- (8) JayaRam, K., "Theoretical and Experimental Investigation of a Copper Vapor Arc with Special Reference to the Spectral Line-Widths," PhD Dissertation, Nagoya University, Nagoya, Japan, 1971.
- (9) Foley, H. M., "The Pressure Broadening of Spectral Lines," Phys. Rev., 69, 11 and 12, p. 616, 1946.
- (10) Mazing, M. A., "On the Broadening and Shift of Spectral Lines in the Plasma of a Gaseous Discharge," Transactions (Trudy) of the Lebedev Physics Institute, USSR, Vol. XV, No. 2, Translated by the Consultants Bureau, New York, 1962.
- (11) Lenz, W., Z. Phys., 25, 299, 1924.
- (12) Weisskopf, V., Z. Phys., 75, 287, 1932.
- (13) Lindholm, E., "Pressure Broadening of Spectral Lines", Arkiv, for Matematik, Astronomi Och Fysk., Band 32A, No. 17, 1945.

- (14) Sobel'man, I. I., Uspekhi Fiz. Nauk, 54, 552, 1954.
- (15) Ovechkin, G. V., and Sandrigailo, L. E., Journal of Applied Spectroscopy, USSR, 10, No. 4, pp. 565-572, 1969.
- (16) Vainshtein and Sobel'man, Optika i Spektroskopiza, 6, 440, 1959.
- (17) Hilsenrath, J., and Klein, M., AEDC-TR-65-58, March, 1965.
- (18) Boyer, D. W., et al, Relative Transition Probabilities and Pressure Broadening Parameters of Copper Atomic Lines, AFFDL-TR-78-82, 1978.
- (19) Miyachi, I., and JayaRam, K., "Theoretical Estimation of the Spectral Line Broadening Constants," ATA PHYSICA POLONICA, A40, 527, 1971.
- (20) Vincenti, W. G., and Kruger, C. J., Jr., Introduction to Physical Gas Dynamics, John Wiley and Sons, Inc., New York, 1965.
- (21) Penner, S. S., Quantitative Molecular Spectroscopy and Gas Emissivities, Addison-Wesley Publishing Co., Inc., 1959.
- (22) Armstrong, B. H., "Spectrum Line Profiles: The Voigt Function," J. Quant. Spectrosc. Radiat. Trans., 7, pp. 61-88, 1967.
- (23) Janson, P. A., and Korb, C. L., "A Table of Equivalent Widths of Isolated Lines with Combined Doppler and Collision Broadening Profiles", J. Quant. Spectrosc. Radiat. Trans., 8, pp. 1399-1409, 1968.
- (24) Corliss, C. H., and Bozman, W. R., "Experimental Transition Probabilities for Spectral Lines of Seventy Elements," NBX Monograph 53, 1962.
- (25) Mason, C., AFFDL-Technical Memorandum, to be published.
- (26) Neel, C. A., and Lewis, C. H., "Interpolations of Imperfect Air Thermodynamic Data, II, at Constant Pressure," AEDC-TDR-64-184, 1964.